CONTENTS

List of Tables

List of Figures

1 Introduction

This chapter begins by presenting the motivation for the research on the behavior of magnetorheolgocial (MR) fluids subject to impact and shock loading. Following the motivation for the research, the objectives, scope and approach are discussed. This chapter concludes by providing an outline of the thesis.

1.1 Motivation for Research

The majority of existing research involving magnetorheolgocial (MR) fluids and devices focuses on systems excited by relatively low velocities and low frequencies. As a result, the characteristics of MR fluid behavior and device design are relatively well understood at low velocities and frequencies. Recently, MR devices have been shown to provide benefits over passive elements in applications where dynamic inputs result in high velocities [1-6]. The research in the area of high velocities and frequencies typically employ an existing device or develop a device based on low velocity design methods. To date, a general understanding of the fluid behavior during high velocity and high frequency applications does not exist. This study investigates the behavior of magnetorheological fluids and basic considerations for MR damper design for high velocity excitations.

1.2 Objectives

Three primary objectives exist for this study,

1. Develop and instrument a drop-tower testing facility,
2. Evaluate the behavior of magnetorheological fluids during impulsive excitation,
3. Provide a basic understanding of how MR damper design relates to the ability to handle inputs that result in high fluid velocities.

The drop-tower facility will be used to impart an impulse to the MR dampers tested. The magnitude of the impulse will be selected to force the fluid to reach high velocities. To capture the event, the drop-tower facility and MR dampers will be instrumented. For the second objective, the behavior of the fluid will be inferred from the results of impacting the two MR dampers. In addition, the goal of the second objective includes deriving

methods to characterize the fluid. The extent of the final objective, relating damper design to high velocity response, will include qualitative considerations for device design.

1.3 Approach and Scope

To understand the behavior of magnetorheological fluids subjected to impulsive excitation, this study included testing two fundamentally different magnetorheological damper configurations. Using a drop-tower test facility, the response of the two MR dampers to impulsive loads was recorded for varying impact velocities. For each impact velocity, five constant currents to each MR damper were explored. Throughout the testing, the mass of the impacting structure was fixed. The test results were used to determine the dynamic response of the MR damper and infer how the fluid was responding.

Since the goal of this study is to understand how the fluid responds to high velocity excitation, it is important to note that no type of control was used for the supply current. Although it has been shown that the dynamic response can be greatly improved by using feedback control, it would be very difficult to separate the dynamic behavior of the fluid from the dynamics of the driving current and time required for the fluid to respond to the driving current. Therefore, for a given impact velocity and current supply to the MR damper, the current was fixed throughout the duration of the impact.

1.4 Outline

This section provides a general description and brief synopsis of each of the following chapters. The next chapter, Chapter 2, begins with a background on magnetorheological fluid technology and the specifics of the two dampers studied in this work. The last section of Chapter 2 summarizes the results of a literature review on magnetorheolgoical fluids and dampers. Chapter 3 focuses on the drop-tower test facility, beginning with the theory of drop-tower testing, and the design and construction of the drop-tower used throughout this study. Chapter 3 concludes with the specifics of the instrumentation of the drop-tower and MR dampers, and the data acquisition system. In Chapter 4, the initial test plan and results from the initial tests are discussed. Modifications to the

instrumentation and signal processing methods used during the initial tests are presented, and the final test plan is developed. The fifth and sixth chapters discuss the results of the final tests on the mono-tube and double-ended MR damper, respectively. Each chapter begins with general descriptions of the response and provides explanations for the observed behavior. The later part of Chapters 5 and 6 include an analysis of the fluid properties during the impact event. Chapter 7 compares the responses of the two damper configurations and summarizes the advantages and disadvantages of each. Chapter 7 also includes general considerations for the design of MR dampers subject to high velocity excitation. The thesis concludes with Chapter 8, which provides concluding remarks and recommendations for future research.

1.5 Contributions

In the area of magnetorheological fluid behavior and magnetorheological damper response to impulsive loading, this thesis offers:

- The design and development of a facility to impact MR dampers
- The relationship between supply current and the following: peak force transmitted, average force transmitted and maximum piston displacement
- The behavior of an accumulator in a mono-tube design during an impact
- The definition of a threshold velocity, where the damping force produced by a MR fluid damper transitions from being independent of to dependent on supply current
- Hypothesizes, including Reynolds number and fluid characteristics, to explain the threshold velocity

2 Background

This chapter provides an introduction to magnetorheological (MR) fluids and an overview of current and future applications of MR fluids. Included are summaries of the development of the two MR dampers used in this study and the results of a literature review.

2.1 Principles of Magnetorheological Fluids

Magnetorheological (MR) fluids are classified as controllable fluids because their rheological properties (elasticity, plasticity, and viscosity) respond to an applied magnetic field. MR fluids consist of a carrier fluid, typically a synthetic or silicone based oil, and ferromagnetic particles (20-50 microns in diameter). In the absence of a magnetic field, MR fluids flow in a linear viscous state. However, in the presence of a magnetic field the particles align and form linear chains parallel to the field, Figure 2–1. The chains act to restrict fluid movement and solidify the suspension. With a properly designed magnetic circuit, the apparent yield stress of the MR fluid will change within milliseconds [7]. The greatest change is typically observed when the magnetic field is normal to the flow of MR fluid. In common MR damper designs, the difference in damping forces may increase by a factor of 10 or more between the passive and fully active states [8].

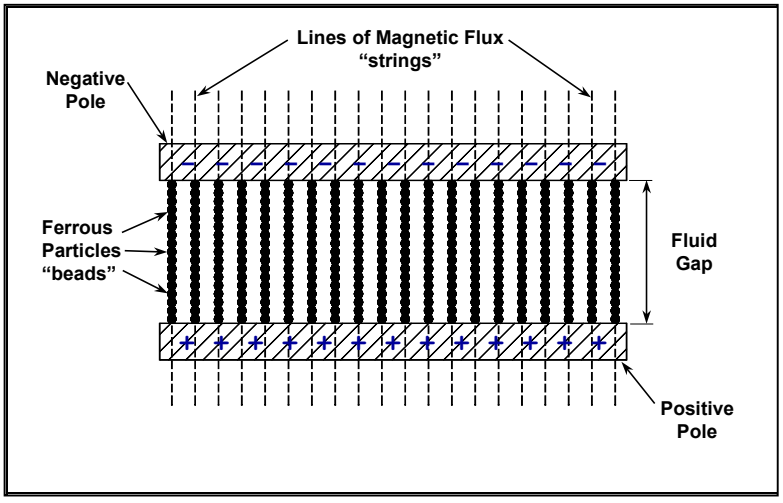

Figure 2–1. Schematic of MR fluid particles aligning with magnetic field [9]

2.2 Applications of Magnetorheological Fluid Technology

Due to their unique properties, MR fluids have been used in optical polishing [10], rotary brakes [11], and semi-active vibration control devices, e.g. shock absorbers and dampers [12-14]. In addition, researchers are exploring the possibility of using MR fluids for intelligent drive shafts [15] and in-vitro blood embolization for cancer treatment [16]. This section gives a brief overview of each of these areas.

2.2.1 Optical Polishing

QED Technologies © manufactures machines that use the MR fluid and an abrasive as a polishing material. A functional diagram of the system, Figure 2–2, shows a lens held above a rotating spherical wheel. By controlling the magnetic field and the position of the lens in real-time, the stiffness and application of the polishing fluid may be optimized to very accurately remove material from the work piece.

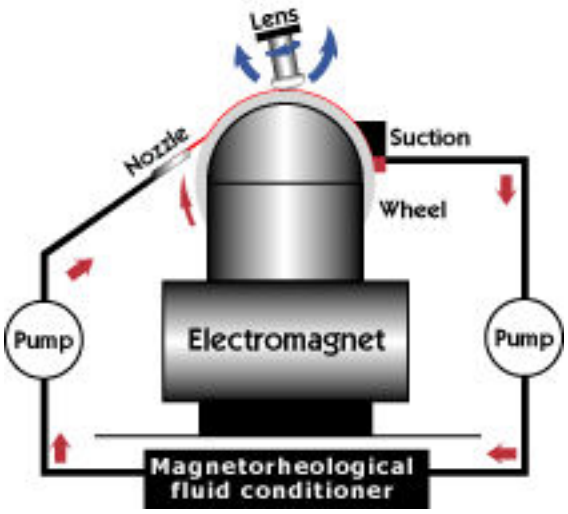

Figure 2–2. Functional diagram of the QED optical polishing system [10]

2.2.2 Rotary Brakes

Lord Corporation© developed a rotary brake, Figure 2–3, that employs the MR fluid in shear mode. The rotary brake has a response time less than 10 ms and requires low power (8 Watts at maximum resistance). Lord markets the brake for precision tension control, pneumatic actuator control, steer-by-wire systems, and similar applications [11].

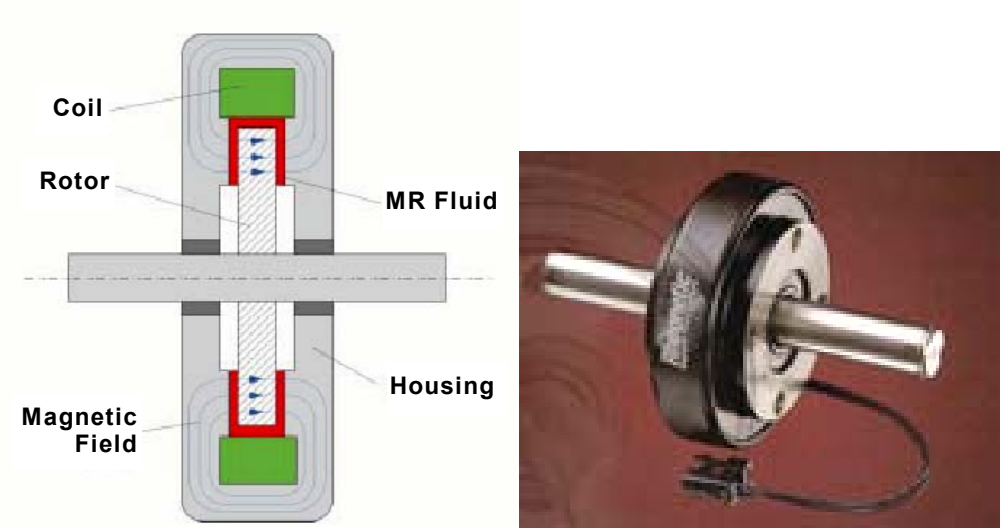

(a) (b)

Figure 2–3. Lord rotary brake (MRB-2107-3) schematic (a) and actual (b) [11]

2.2.3 Magnetorheological Dampers

The majority of MR fluid technology appears in MR dampers. MR dampers find applications in small devices, for example above the knee prosthetics [17], to large systems, such as earthquake mitigation in civil structures [18]. Three common configurations of MR dampers exist: mono-tube, twin-tube and double ended.

Figure 2–4. Prosthetic MR damper and 180 kN double-ended MR damper for civil engineering applications [19]

The mono-tube MR damper, Figure 2–5 (a), has only one volume of MR fluid and an accumulator to accommodate the change in volume due to the additional volume displaced as the piston shaft enters the housing. Mono-tube dampers are the most common configuration. The twin-tube MR damper, Figure 2–5 (b), has two concentric tubes connected with a valve. The valve allows for MR fluid to flow from the inner to the outer tube to adjust for piston displacement. The third common configuration is the double-ended design, Figure 2–5 (c). Because the piston shaft is the same diameter throughout the body, double-ended dampers do not need to account for changes in volume.

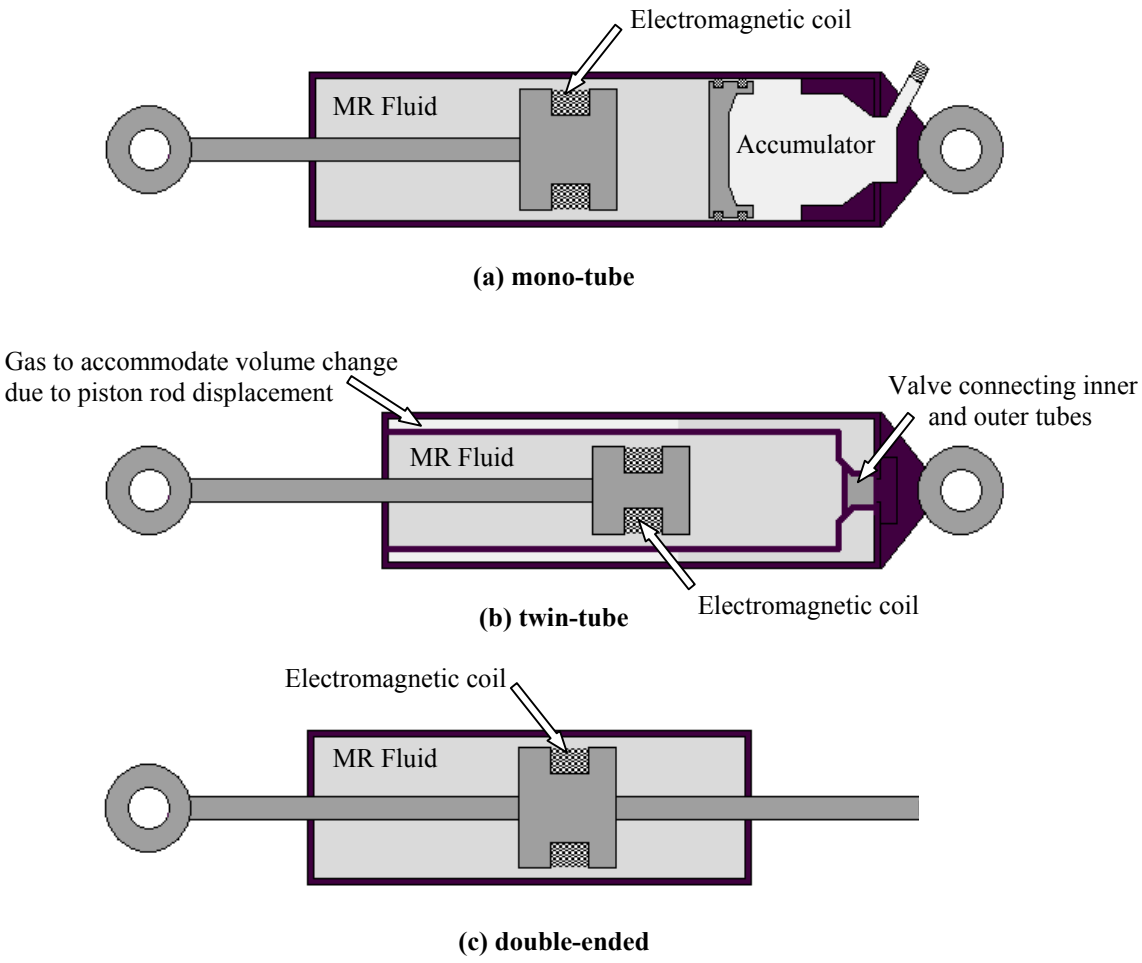

Figure 2–5. Cross-sections of three common configurations for MR dampers

Common MR damper designs also include variations in the number of activation regions, also referred to as the number of stages. Activation regions are the areas where the MR fluid passes through a magnetic field. Each of the dampers in Figure 2–5 employ

one electromagnet coil, and therefore are single-stage designs. Figure 2–6 shows a three-stage, double-ended design for civil engineering applications. The magnetic flux lines are sketched in the detail accompanying Figure 2–6.

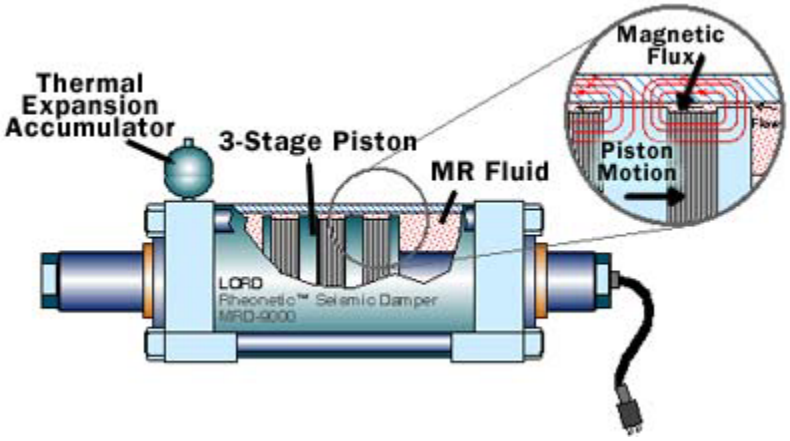

Figure 2–6. A Three-Stage, Double-Ended MR Damper for Structural Damping [18]

Three common modes of operation exist in MR damper designs: squeeze, shear, and valve mode, diagramed in Figure 2–7. Squeeze mode MR dampers offer the greatest difference in damping force for a given change in magnetic flux. However, the amount of displacement achievable for a squeeze mode MR damper is significantly less than the other modes. The shear mode is used to control damping in rotary applications. An example of a shear mode rotary damper is the MR brake developed by Lord Corporation (see Section 2.2.2). The valve flow mode is the most common mode used for MR dampers. The two dampers studied in this work operate in the valve flow mode.

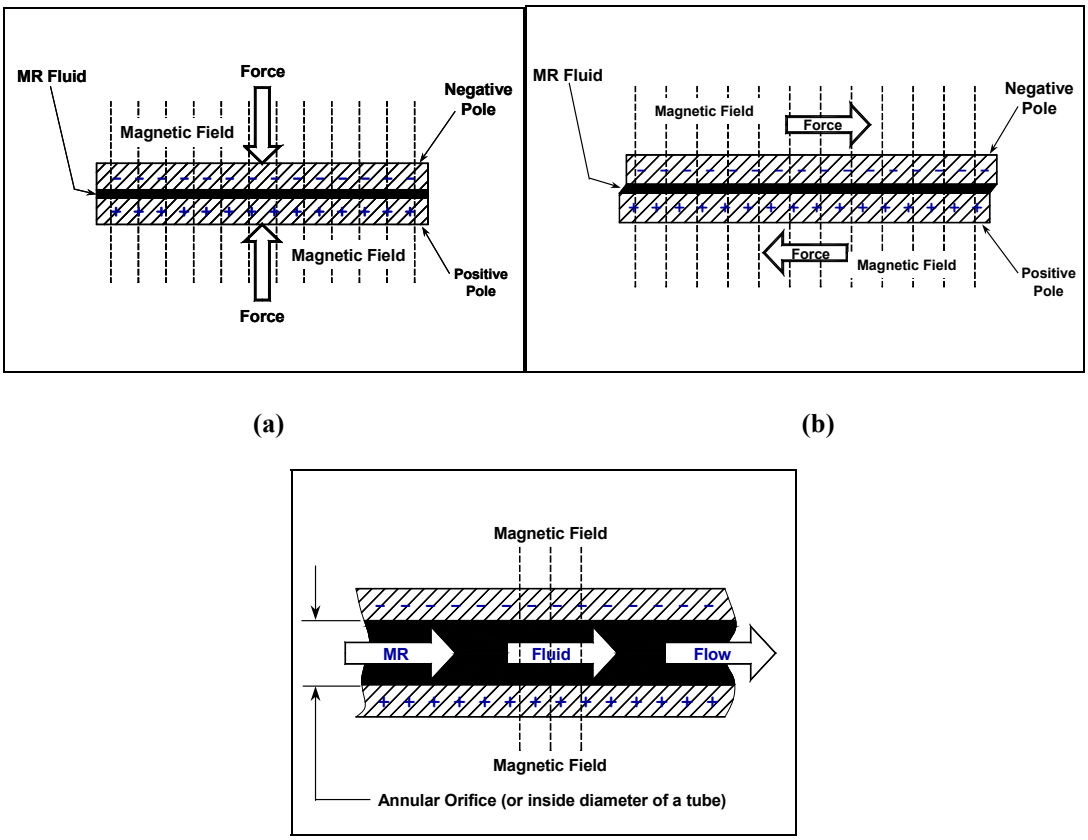

Figure 2–7. Three common modes of operation for MR fluid dampers; (a) squeeze mode; (b) shear mode; and (c) flow mode [9]

Figure 2–8 shows an example of the typical relationship between damping force and velocity for valve mode dampers. As the applied magnetic field is increased, the damping force increases until a saturation point is reached. The saturation point is defined by the point where increasing the magnetic field fails to produce an increase in the damping force. For a properly design magnetic circuit, the difference between the off-state and saturation damping force may be as high as a factor of 10 or more [8].

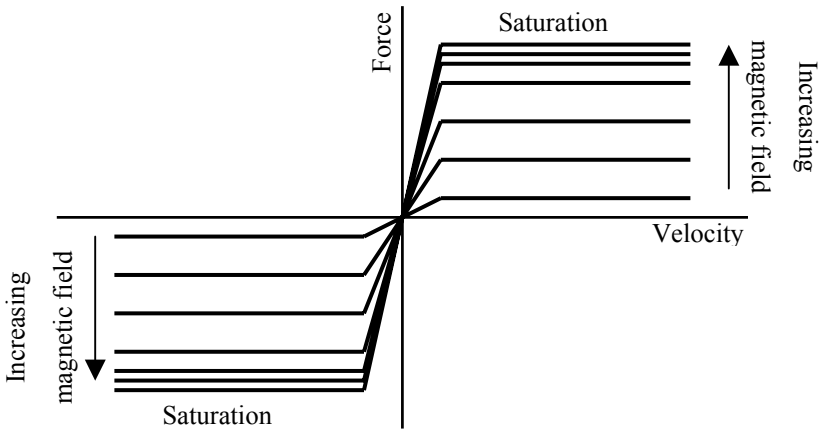

Figure 2–8. Relationship between damping force and applied magnetic field

2.2.4 Intelligent Drive Shafts

Dana Technology© is currently developing magneto-rheological center bearing brackets to allow real-time adjustments of the brackets within the driveline suspension system. By controlling the stiffness and damping of the brackets, Dana claims, "it is no longer necessary to sacrifice high-speed noise, vibration and harshness for low-speed rigidity and strength," [15].

In addition to the center bearing brackets, Dana Technology mentions possible future applications of MR fluids. They state that the MR fluid could be used in conjunction with ABS wheel sensors to create a variable locking axle differential, and for fully electronic disconnect capabilities in four-wheel drive transfer cases.

2.2.5 *In-vitro* Blood Embolization for Cancer Treatment

Just like healthy organs, cancerous tumors receive their nutrients from blood vessels. Liu et. al. have proposed a method to starve the cancerous tumors by blocking blood flow to the tumor with magnetorheological fluids [16]. Using a simulated blood network of silicone tubes, they were able to show that MR fluids are capable of producing sealing strengths that would block typical arteries. This is a very new application of MR fluid technology, and while showing promise is still in its early stages of development.

2.3 Development of the Magnetorheological Dampers in this Study

This section presents the specifications and development of the two dampers used in this study. Both of the dampers were designed and built by James Poynor as part of his thesis work [9]. One damper was designed to replace a stock Ford Expedition front damper, Figure 2–9(a), and the other was designed for recoil studies with a 50-caliber rifle, Figure 2–9(b). For simplicity, the Ford Expedition damper and the gun recoil damper will be referred to as the mono-tube MR damper and the double-ended MR damper, respectively, in the remainder of this thesis.

(a)

(b)

Figure 2–9. The two MR dampers studied: mono-tube (a) and double-ended (b)

The Ford Expedition damper is a two-stage, mono-tube with nitrogen accumulator configuration and the gun recoil damper is a single-stage, double-ended design. The number of stages refers to the number of regions where the fluid is subject to a magnetic field (activation regions). For example, the damper shown in Figure 2–10 is a two-stage design. Both the mono-tube and double-ended dampers operate in the valve mode and contain MRF-128 TD fluid from Lord Corporation. Additional information and detailed drawings are available in James Poynor's thesis [9].

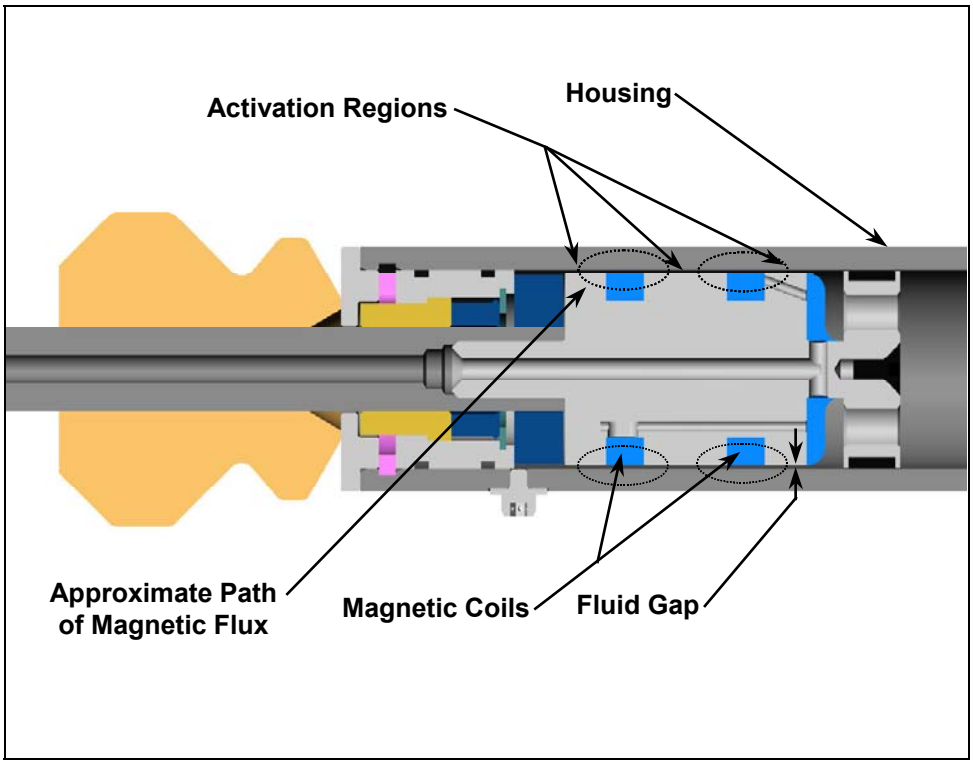

Figure 2–10. Activation regions in a two-stage design [9]

2.3.1 Mono-tube Ford Expedition Damper

The Expedition damper is a two-stage piston design. Figure 2–11 shows a cross sectional view of the Expedition damper. The two coils are constructed using 24-gauge magnet wire wrapped around a paper based phenolic coil form. The mono-tube design includes a nitrogen accumulator to reduce the chance of MR fluid cavitation and accommodate for changes in volume due to the piston rod entering the housing. During this study the nitrogen accumulator was pressurized to 185 psi. A complete list of specifications is provided in Table 2–1.

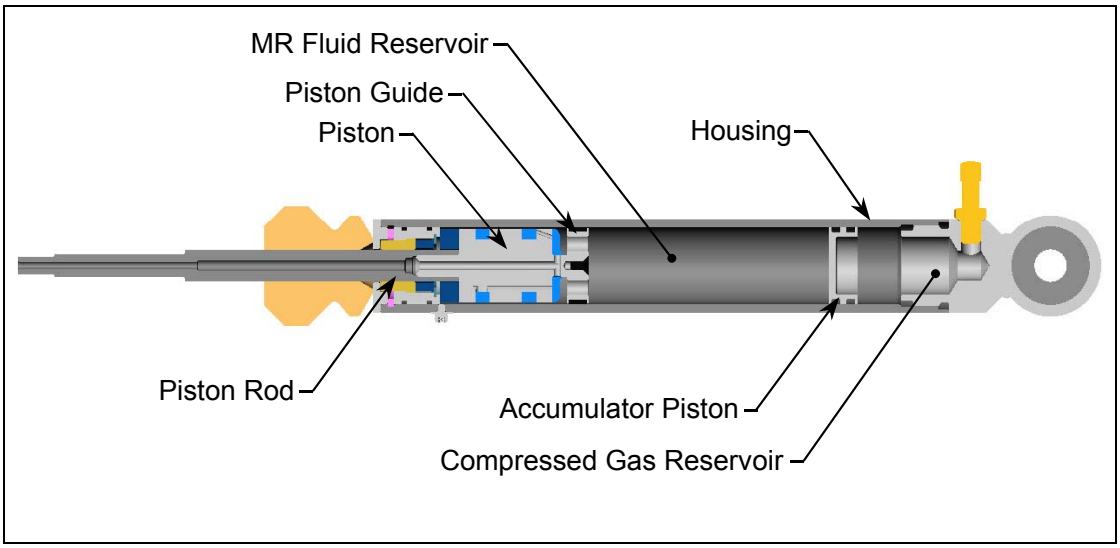

Figure 2–11. Expedition MR damper section view (Adapted from [9])

Table 2–1. Design specifications for the Ford Expedition damper

Parameter	Value	Parameter	Value
Number of coils	2	Coil inner diameter	0.978 in
Wire gauge	24	Piston outer diameter	1.344 in
Number of turns per coil	48	Gap	0.015 in
Resistance per coil	0.58 Ω	Housing wall thickness	0.125 in
Coil wiring	Parallel	Total stroke	4.1 in
Total resistance	0.29 Ω	Accumulator pressure	185 psi

2.3.2 Double-ended Gun Recoil Damper

The gun recoil damper is a single-stage, double-ended design. As shown in Figure 2–12, piston rods exit both the front and rear of the housing. During operation the MR fluid flows around the piston through the activation regions. The design uses one coil of 20-gauge magnet wire wrapped approximately 230 turns. The outer housing was machined from 1018 steel. A complete list of specifications is given in Table 2–2.

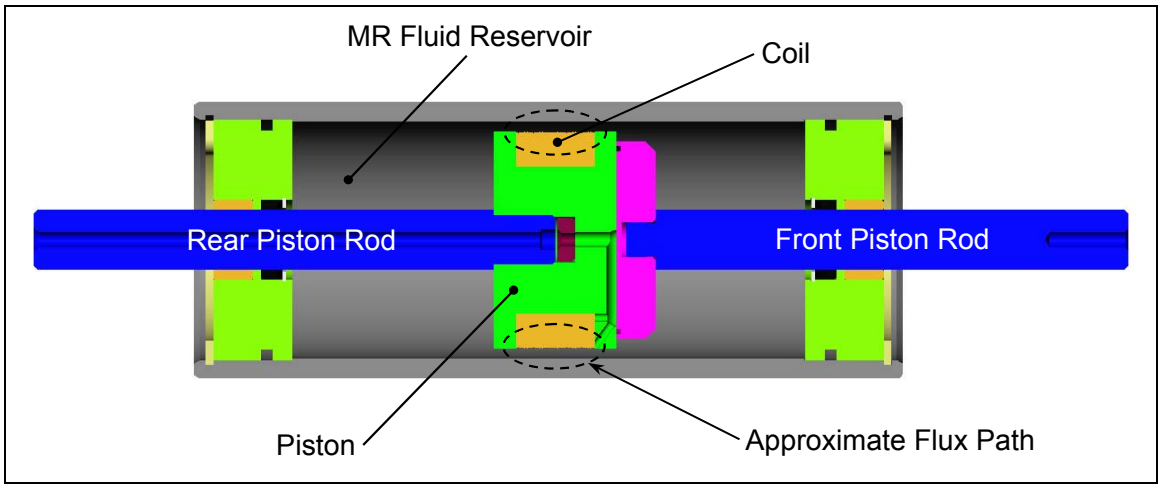

Figure 2–12. Double-ended gun recoil damper section view [9]

Table 2–2. Design specifications for the gun recoil damper

Parameter	Value	Parameter	Value
Number of coils	1	Coil inner diameter	1.870 in
Wire gauge	20	Piston outer diameter	2.77 in
Number of turns per coil	~230	Gap	0.115 in
Resistance per coil	2.13 Ω	Housing wall thickness	0.25 in
Coil wiring	N/A	Total stroke	4.4 in
Total resistance	2.13 Ω	Accumulator pressure	N/A

2.4 Literature Review

To gather information about studies related to the focus of this work, a literature search of journal articles and websites was performed. Searching for keywords was conducted using the Comprehensive Engineering Index (Compendex database), INSPEC, SCIRUS and the web search engine Google.

This section begins with an explanation of the keyword search structure. The results of the review are then grouped by subject and summarized.

2.4.1 Keyword Search Structure

Part of the motivation for this work was because of the limited published research relating physical design to performance during impact loading. Therefore, the search included material that did not directly discuss magnetorheological fluids, for instance the keyword combination impact and damper. The keyword structure was applied to each search database. The results from the Compendex search, which produced the majority of results, are presented in Table 2–3.

Table 2–3. Keyword search diagram for magnetorheological literature: Compendex

	-	Design	impulse	impact	transient	shock	model	damper
magnetorheological	337	63	0	5	4	20	108	108
Magneto rheological	101	20	0	1	1	8	39	45
Magneto-rheological	101	20	0	1	1	8	39	45
MR	6201	509	7	66	40	49	948	108
Damper	4458	1251	25	255	263	249	1369	-
Damping	36454	6643	391	1192	1780	956	9220	-

After conducting the literature search, it was clear that some combinations of keywords were too general and produced too many results. For example, the combination of damping and model produced 9220 papers. In these instances, the search results were discarded. In addition, when the abbreviation MR was used, search engines often brought up papers about Magnetic Resonance Imaging (MRI). Lastly, magneto rheological and magneto-rheological produced the same results in Compendex, but not in the other search engines.

The literature search reaffirmed that very little published work existed on magnetorheological devices subjected to impact and shock loading. The results of the literature review were grouped into four main subject categories: modeling, design, and experimental studies of MR dampers, and impulsive loading of any type of damper. The papers are summarized in the following sections.

2.4.2 Modeling of Magnetorheological Dampers

Models of magnetorheological dampers are used to describe the dynamic behavior of MR dampers, for instance the relationship between damping force, velocity and supply current. Two general approaches to describe the behavior of MR dampers exist, namely, modeling experimentally observed behavior, and deriving the behavior based on fluid mechanics analysis. Usually papers that present models also include experimental results, which are used to determine model parameters and/or validate the proposed model. The majority of models are designed by studying the experimental response of MR dampers subject to sinusoidal loading and assuming the fluid is flowing in a quasi-steady flow.

Three of the more common models for recreating experimentally observed behavior are the nonlinear Bingham plastic, nonlinear biviscous and nonlinear hysteretic biviscous, shown in Figure 2–13 [20, 21]. The dashed lines in Figure 2–13 represent the response predicted by the models and the solid line is the experimentally observed behavior. It is important to point out that the force-velocity behavior has only been studied up to piston speeds of about 30 in/s. The force-velocity behavior above these piston speeds has not been explored either experimentally or theoretically. The parameters for these models depend on supply current and are determined by experimental results. The nonlinear Bingham plastic model assumes that the fluid does not move until the yield force, F_y, is exceeded. After which point, the fluid is assumed to behave as a linear viscous fluid. The nonlinear biviscous expands upon the Bingham model by incorporating a pre-yield linear damping. In the case of sinusoidal excitation, MR dampers exhibit hysteresis and to capture this behavior the nonlinear hysteretic biviscous model was developed.

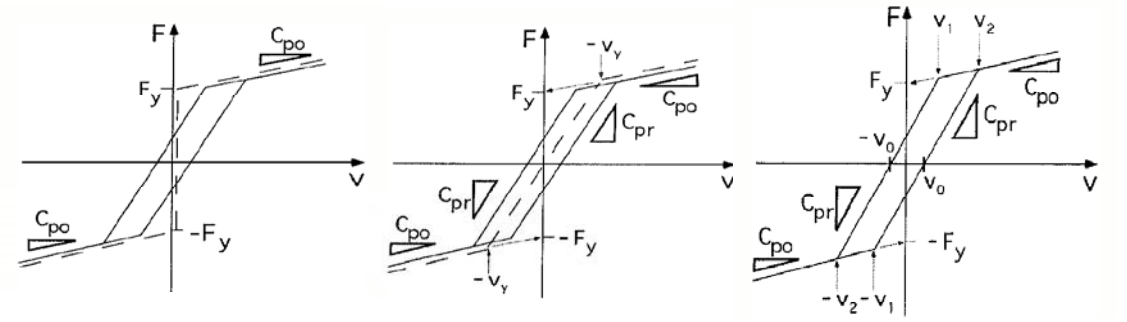

Nonlinear Bingham plastic **Nonlinear biviscous** **Nonlinear hysteretic biviscous**

Figure 2–13. Nonlinear damper models, model force vs velocity is the dashed line and experimentally observed behavior is the solid line [20]

Snyder et al. compared the three common nonlinear models and expand upon another model, the nonlinear-viscoelastic plastic (NVEP) model [20]. The NVEP model divides the damping force into pre-yield, yield and post-yield components that are summed to predict the force output. In addition the NVEP model, is piecewise smooth in velocity. After identifying the parameters for each of the four models from experimental data, performance criteria are established and comparisons between the four models are presented. The theoretical energy dissipation and ability to reconstruct the hysteresis cycle were predicted significantly better by the NVEP model than the other three.

A different method to capture hysteretic cycles is the use of the Bouc-Wen model. Spencer et al. present the basic Bouc-Wen model and additional modifications to the model [22]. Their work also includes a model to account for the relationship between input voltage and the MR fluid reaching equilibrium. Yang et al. expand upon the model presented by Spencer et al. by modeling the magnetic circuit and a current driver [18]. To reduce damper response times, Yang et al. conclude that the electromagnetic coils should be configured in parallel and the voltage available to the current driver should be as high as possible. In addition, to reduce the influence of the residual magnetic effect present when the current needs to be reduced to the coils, they show that driving the current in the opposite direction significantly improves the response time. For the MR damper they studied, the current driver is able to reduce the time required to supply a given current by a factor of 15 when compared with a constant voltage step input.

Another technique to model MR fluid behavior is based on fluid dynamics. One such technique is based on the Herschel-Bulkley constitutive equation. Wang et al. take compressibility effects into account and provide a detailed development of the equations governing the model [23]. In addition, design parameters are related to performance. They conclude by validating the model with experimental results.

To understand the response time of MR and electrorheological (ER) fluids, Choi et al. develop a number of dimensionless criteria for MR and ER fluid flow through parallel plates [24]. Based on analytical simulations and experimental results, they conclude that MR fluids are better for applications where high controllable performance requirements are desired. However, they point out that MR fluids do not respond as fast as ER fluids for equivalent configurations.

2.4.3 Design of Magnetorheological Dampers

The papers on the design of magnetorheological dampers may be grouped into two sub-categories. The first sub-category is designs that employ varying models for optimal selection of design parameters. The second sub-category is concerned with designing new configurations for MR dampers.

In the first sub-category, Gavin et al. relate a number of MR damper design parameters to the time constant of the device and the electric power consumption [8]. The design was constrained by force capacity (defined by forces at piston velocities of 2 and 30 cm/s {0.79 and 11.8 in/s}), size and electrical characteristics. After defining the constraints, an optimization was run to determine the optimal flow gap, length of the poles, number of spools, number of windings in each spool, wire gage, coil inner diameter and magnetic flux density in the flow gap. The optimal design was then constructed and experimental tests were performed to validate the model. In addition, they present an algebraic model relating output force to applied voltage, and piston position and velocity. The model is easily rearranged to compute the required voltage for a desired damper force.

Carlson et al. provide a comprehensive overview of basic design considerations for MR dampers and test the ability of a MR damper to control a model of a three-story building during a simulated earthquake [25]. After discussing basic properties of MR

fluids, they present dimensionless equations for the pressure gradient and stress of an MR fluid in valve mode, equations to calculate the minimum active fluid volume and guidelines for power requirements. The latter half of the paper is concerned with the control of the vibrations in the model building, and the development of a 20-ton damper designed for full-scale investigations into seismic control.

In the second sub-category, Kelso develops a MR fluid damper that offers minimal cost and simplicity of design [26]. Four parameters are weighed in the design, including the availability of materials, inclusion of commercially off-the-shelf components, serviceability and maintenance, and zero-field damping adjustment. After establishing the device design, equations for the optimal design of the electromagnetic circuit are presented. The paper concludes with experimental results of the final design.

Lindler et al. present a mono-tube, single-stage magnetorheological damper with a gap that may be adjusted to produce a uniform or non-uniform gap between the housing and piston [12]. Comparisons between the effects of the type of gap on the ability of the magnetic field to control the force-velocity characteristics are presented. They note "the uniform gap primarily adjusts the yield force of the shock absorber, while the non-uniform gap allows for control of the post-yield damping," [12].

2.4.4 Experimental Studies of Magnetorheological Dampers

As mentioned earlier, the majority of design and modeling papers also include experimental results for validation of results and model parameter selection. This section includes papers that focus primarily on experimental results and may include models to fit or predict the observed behavior.

Sunakoda et al. present the force-displacement results for two MR fluid dampers that employ a bypass flow system, one with a capacity of 2 kN and the other 20 kN [27]. They conclude that the magnitude of the damping force is controllable by the input current; however, there is a point where supplying additional current does not yield an increase in the damping force. The involution model is fit to the data to simulate the force velocity relationship.

Muriuki et al. explore the relationship between the magnetic field orientation and actuator geometry by testing two different types of cylinder configurations [28]. The

same damper geometry was used, however, two different fluid flow rates and flux orientations were tested. The damping forces were compared and conclusions about the importance of the proper orientation of the magnetic field were stated.

2.4.5 Impact Vibration and Shock Loading of Dampers

The first two papers in this area include studies on damping devices that do not use magnetorheological fluids to mitigate impact loads. The remaining studies investigate magnetorheological fluids and devices for isolating systems from impact and shock loading.

Bajkowski presents modeling techniques for the energy accumulation and dissipation cycles of shock absorbers with dry friction subject to impact loads [29]. He notes that for modeling purposes shock absorbers may be divided up into elastic and dissipative elements. The paper provides a very good background on different techniques to model hysteresis cycles and general considerations for modeling dampers.

Tanaka et al. developed a semi-active damper for impact vibration control [30]. The paper begins by presenting the inability of passive damping elements, which are designed for steady-state excitation, to mitigate impulsive loads. They then divide semi-active dampers into three categories based on which element is controllable, namely, damping coefficient, spring rate and initial conditions on the damping mass. Their semi-active damper falls into the third category and is realized by releasing the damping mass from an initial displacement. The damping mass is attached to the mass to be isolated by springs and a tunable damping element. By theoretically varying initial conditions, damping ratio and release times (relative to the initial impact) they present the ideal design for this semi-active damping method. The paper concludes with validating the theoretical design with experimental results.

For the papers on MR dampers, the first paper reviewed, by Ahmadian et al., investigates the ability of a double-ended MR damper to control shock dynamics using a 50-caliber rifle [1]. This paper includes the force velocity characteristics of the MR damper studied and preliminary results for the ability of the MR damper to mitigate the recoil forces associated with firing the 50-caliber rifle. The damper dimensions and design are related to the ability of mitigating impulsive loads.

The other studies by Ahmadian et al. focus on using MR dampers in a fire out-of-battery (FOOB) sequence for a 105mm cannon [2, 3]. The cannon is modeled as a single degree of freedom mass-spring-damper system. The damping element is modeled first as a conventional hydraulic damper and then as a controllable MR damper. A basic control logic for the MR damper is presented and the advantages of using a MR damper over a hydraulic damper are then discussed.

Tanner presents an isolation system that employs MR dampers and air springs to develop a shipboard mount capable of isolating components from a variety of inputs [4]. The system is modeled using a modified Bouc-Wen model for the MR damper in parallel with an air spring model. Using the model, two different control approaches are developed. The system was built and a shock input to the base of the system was experimentally simulated. The results show that the system drastically reduces the force transmitted to the isolated mass.

Wahed et al. investigate the dynamic performance of MR and electrorheological (ER) fluids when subjected to impulsive loads [5, 6]. The ER fluid was used in a squeeze flow mode device and the MR device was a Lord Corporation RD-1005-3 vibration absorber. A test rig that is capable of releasing either 0.221 and 1.309 kg {0.487 and 2.886 lb} from heights between 6.5 and 16.5 cm {2.56 and 6.50 in} is used to impact the MR and ER devices. For both devices, the force transmitted is shown to increase for increasing field strengths. Wahed et al. conclude that both "ER and MR fluid technology are capable of controlling forces and movements in structural components subjected to impulsive or dynamic loading conditions due to the fast response times of the fluids."

It is important to point out that the impact heights and drop-mass studied by Wahed et al. are both orders of magnitude smaller than the impact heights and drop-mass studied in this thesis.

3 Experimental Setup

This chapter includes the theory, design and instrumentation of the experimental setup. The first section discusses the theory behind drop-tower testing. Additionally, the equations governing the impact energy, velocity and dissipation are introduced. The next section presents the actual design, key components and construction. The chapter concludes with a section on the instrumentation and data acquisition system used during the tests.

3.1 Drop-Tower Theory

Drop-tower testing is an effective and inexpensive means to study the dynamic response and energy absorption of components that are subjected to impulsive loads. The principle behind a drop-tower is to use a guided, falling mass to strike a test specimen. By varying release heights and drop masses, the kinetic energy, impact velocity and momentum are easily controlled. For a drop mass guided on lubricated cables, with sufficient clearance, frictional effects and drag may be assumed negligible [31, 32]. Assuming the falling mass is initially at rest, the relationship between kinetic, *KE*, and potential energy may be derived as,

$$KE = \tfrac{1}{2} mv^2 = mgh \tag{3.1}$$

where m is the falling mass, v is impact velocity, g is gravity and h is the difference between the release and impact heights. Solving Equation (3.1) for velocity yields the relationship between impact velocity, v, and height,

$$v = \sqrt{2gh} \tag{3.2}$$

Once the falling mass contacts the test specimen, the energy absorption/dissipation phase begins. A free body diagram of a damper (test specimen) is shown in Figure 3–1. Provided the drop mass remains in contact with the specimen, the energy transferred, *E*, during this event is,

$$E = \int_0^{\delta} F(x)dx \tag{3.3}$$

where $F(x)$ is the force provided by the damper and δ is displacement after the event. Furthermore, by equating Equations (3.1) and (3.3) an average absorption/dissipation force, $\overline{F}$, may be computed from,

$$\overline{F} = mg\left(\frac{h}{\delta}\right) \tag{3.4}$$

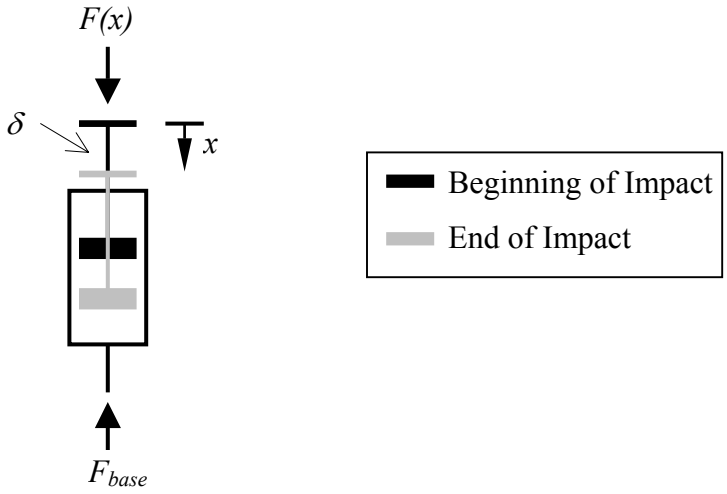

Figure 3–1. Free body diagram of damper (test specimen) during energy absorption phase

3.2 Drop-Tower Design and Construction

The first step in building the drop-tower was to decide on an acceptable nominal drop mass. To maximize the versatility of the structure for future tests, we chose to minimize the drop mass. After a number of iterations, a design that offered both strength and minimum mass, shown in Figure 3–2, was chosen. The structure has a nominal mass of 55 lbs, which can be increased up to 500 lbs by adding steel plates. To minimize the effect of friction, $\frac{1}{2}$ inch steel cable and $\frac{5}{8}$ inch inner diameter tubes were used to guide the falling mass. The exact dimensions and detailed drawings are included in Appendix C.

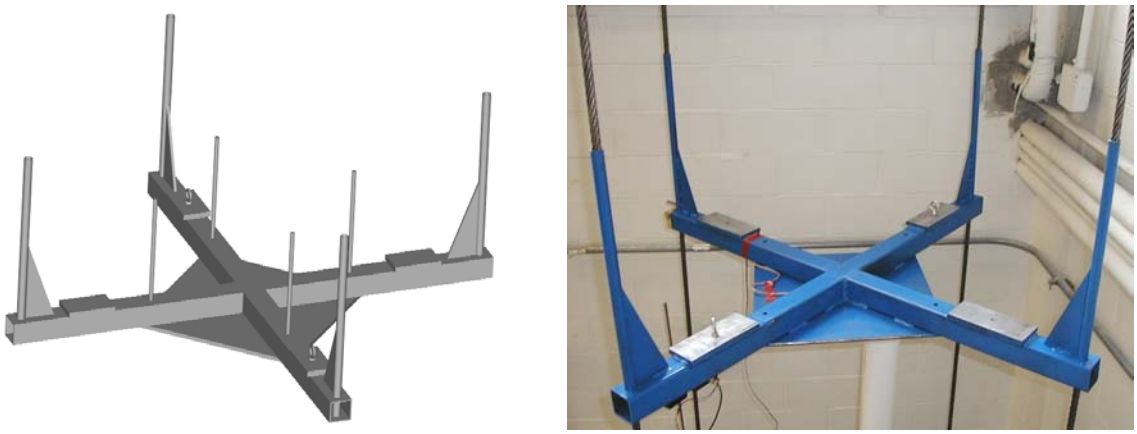

(a) **(b)**

Figure 3–2. Drop mass design (a) and actual structure (b)

The location determined for the structure limited the maximum drop height to 96 inches, corresponding to a maximum velocity of 260 inches per second. The completed drop-tower, Figure 3–3, uses cables to guide the drop-mass. To keep the cable from interfering with the impact area, the cables are guided around pulleys and tensioned using turn buckles. A 2-ton hoist is used to lift the drop mass. Lastly, a safety barrier constructed out of 1/8th inch Plexiglass encloses the base of the test area (not pictured).

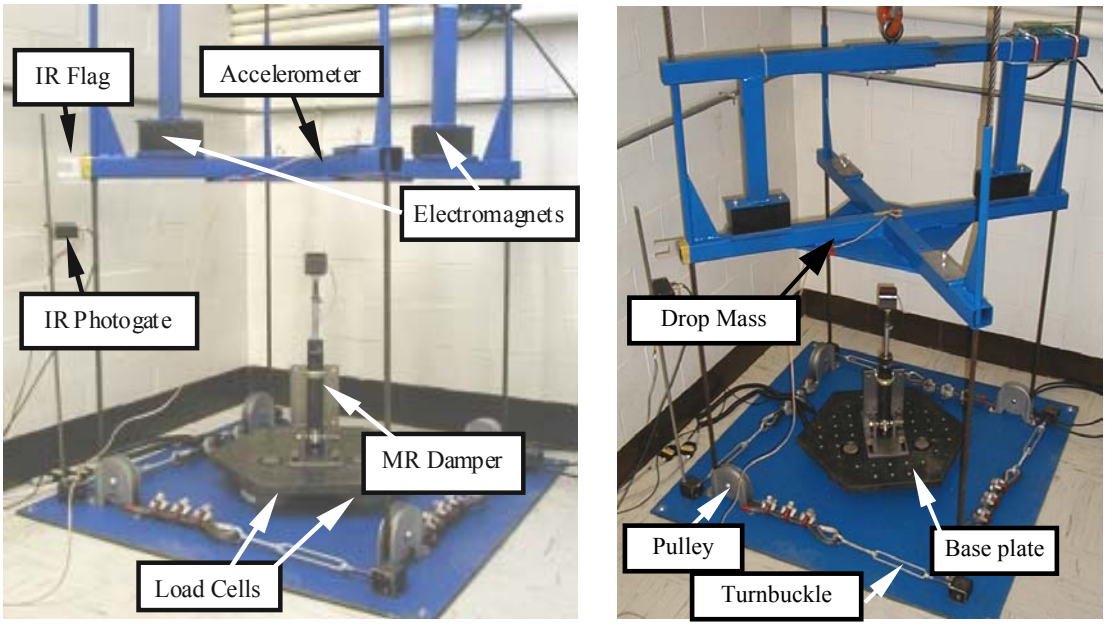

Figure 3–3. Drop-tower test facility

3.3 Drop Tower Instrumentation and Signal Processing

This section includes details of the four types of instruments used to capture the event: the accelerometers, infrared velocity transducer, LVDT and load cells. In addition, the location of each of these instruments is discussed. Power to the load cells, accelerometers, and infrared velocity transducer was provided by a 12-Volt DC (VDC) regulated Astec power supply. This section concludes with the details and setup of the SONY data recorder and computer interface.

3.3.1 Accelerometer Specifications and Experimental Setup

Accelerometers were located on the drop-mass, damper piston and the base-plate as shown in Figure 3–4. Because of the high accelerations expected, Motorola Micromachined Accelerometers +/- 250 g (MMA1200D) were used to capture the impact event. A regulated supply voltage of +5 volts was provided by using a LM317 voltage regulated circuit connected to the Astec 12 VDC supply. The accelerometers also required a signal conditioning circuit included in Appendix C.

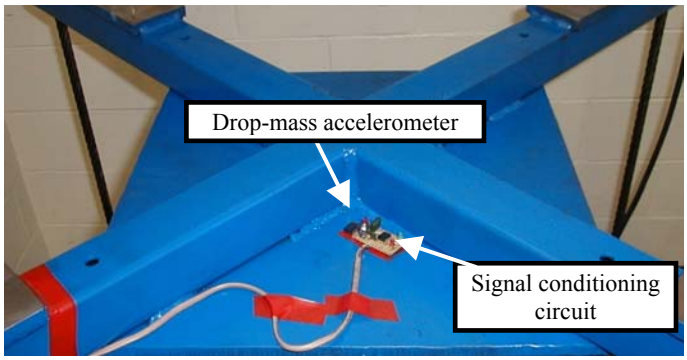

(a)

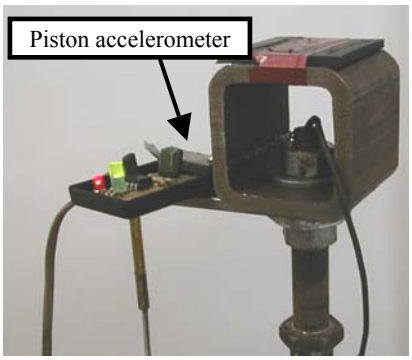

(b)

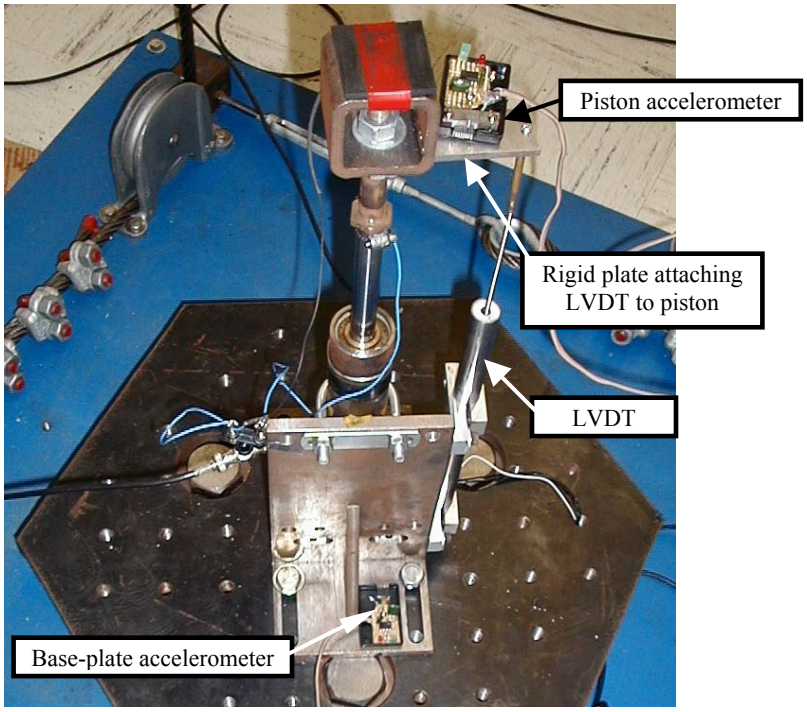

(c)

Figure 3–4. Location of drop-mass (a), piston (b), and base-plate (c), accelerometers

The accelerometers were mounted to the structure using a 90-secound, quick-drying epoxy. While this was sufficient for the drop mass and base-plate, the damper piston experienced such a large shock that the epoxy would not hold. To fix this problem, three holes were tapped into the rigid plate connecting the damper piston and LVDT core. The front two holes were used in combination with a small piece of steel to clamp the accelerometer to the rigid plate. The third hole was used to secure the plastic

housing for the signal conditioning circuit to the rigid plate. Lastly, holes were tapped into the plastic housing to secure the signal conditioning circuit board down.

As a check on the accelerometers, the signal from the drop mass was integrated up to the point of impact and compared with the impact velocity calculated from the infrared circuit. The integrated accelerometer signals were found to agree within 5%.

3.3.2 Infrared Velocity Transducer

To determine the velocity just before the impact, an infrared (IR) photogate trigger was constructed, Figure 3–5 and Figure 3–6 (a). By using a "flag" of know dimensions, Figure 3–6 (b), the signal from the IR trigger may be used to calculate the amount of time the flag required to travel past the IR detector. The flag was designed to trigger the IR circuit twice. Velocities based on the amount of time between the two leading edges and two trailing edges were computed, compared and averaged to determine the velocity just before impact. As an additional check on the impact velocities, Equation (3.2) was used to determine the theoretical impact velocities. The IR circuit velocities were 5-10% less than the theoretical velocities due to cable friction and air drag.

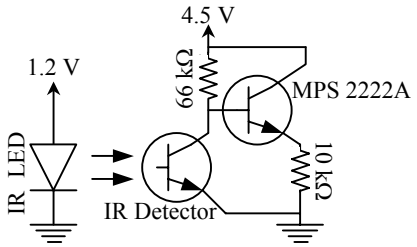

Figure 3–5. Infrared photogate circuit for computing impact velocity (modified from [33])*

*A component list is included in Appendix C

Since the two dampers tested were slightly different heights, the IR circuit was mounted on a threaded rod. To adjust the IR circuit to trigger just before the impact, a digital voltmeter was connected to the circuit and the drop mass was lowered to just barely touch the damper. The height of the IR circuit was then varied until the trailing

edge of the IR flag was just beyond the IR circuit, indicated by a near zero output on the voltmeter.

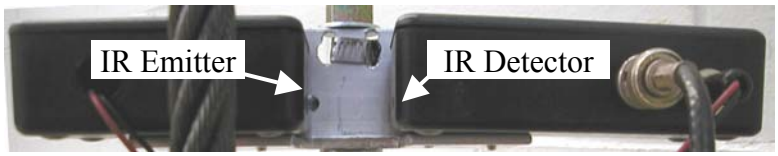

(a)

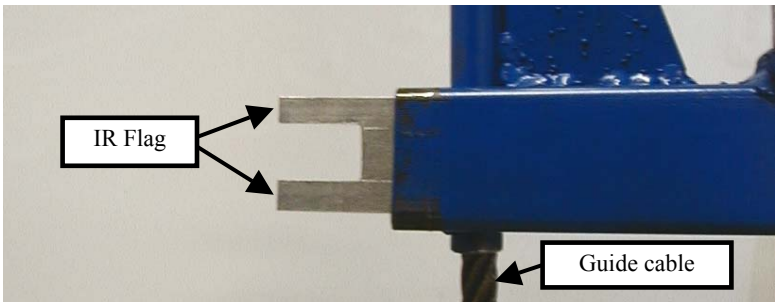

(b)

Figure 3–6. Infrared photogate for impact velocity calculations (a) and flag (b)

3.3.3 LVDT Specifications and Experimental Setup

For monitoring the displacement of the MR damper piston during impact, a Macrosensors' DC-750 series LVDT was rigidly attached as shown in Figure 3–7. The power supply was a regulated ± 15 VDC from Macrosensors. The sensitivity of the LVDT was 5.21 volts per inch. As a check on the LVDT signal, the derivative was taken and the peak velocities were compared to the impact velocity.

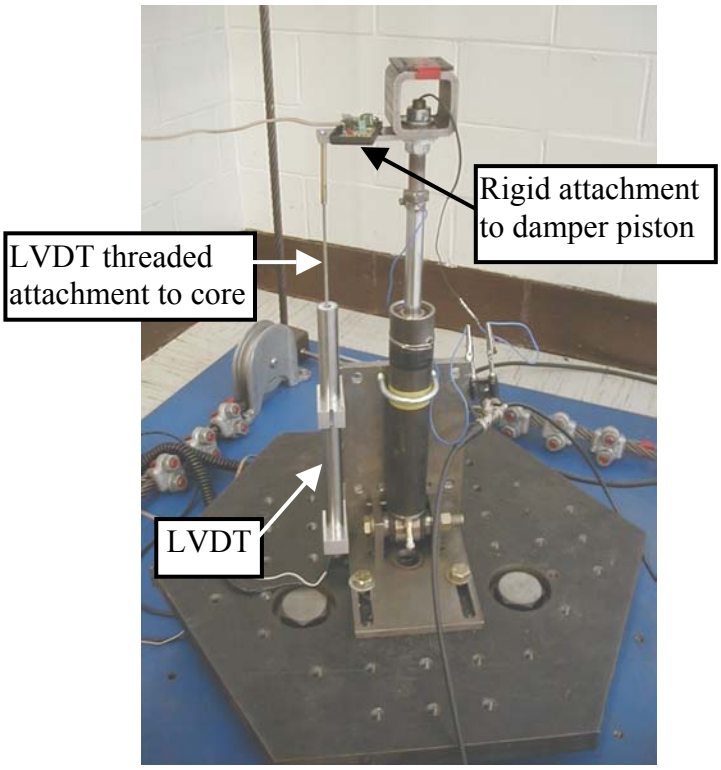

Figure 3–7. LVDT attached to the damper piston

3.3.4 Load Cell Specifications and Experimental Setup

The force transmitted to the base was monitored with three Futek L2900, 20000 lb load cells. To amplify the outputs, Futek JM-2 Amplifer modules were connected to the load cells. The load cells were arranged in an equilateral triangle pattern and centered under the hexagonal base plate. The base plate was constructed from a 1½ inch thick steel hexagon to distribute the static load evenly between the three load cells.

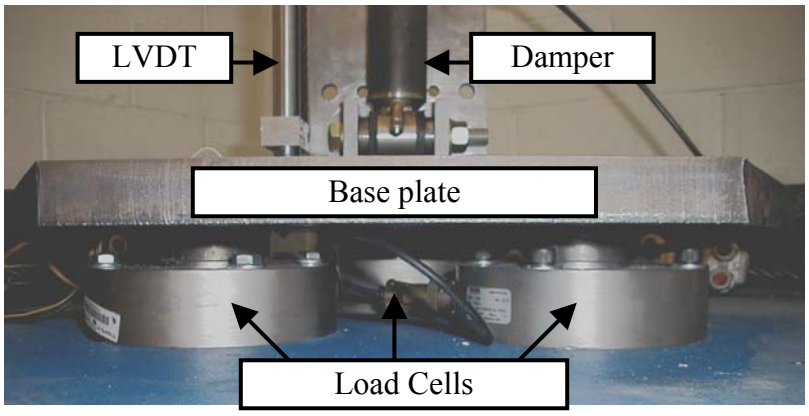

Figure 3–8. Three Futek L2900-20000 lb load cells were placed underneath the base plate

3.3.5 Sony Data Acquisition System and Software Specifications and Setup

The data acquisition system was a Sony Precision Technology PC316AX data recorder, Figure 3–9. Signals from the accelerometers, IR circuit, LVDT and load cells were sampled at 12 kHz and transferred directly to the computer using the PCIF-5 interface. The PCIF-5 interface, shown in Figure 3–10, allowed remote control of the data recorder through a COM port and transmitted data to the computer parallel port (configured in EPP mode).

Figure 3–9. Sony PC216AX data recorder

Figure 3–10. PCIF-5 interface for controlling and transferring data to computer

The computer was remotely operated and the signals were recorded to the computer using Sony PCScanII software. From PCScanII, the data was exported to Matlab compatible formats for analysis.

4 Experimental Procedures and Initial Test Results

This chapter presents the design of the initial test matrix, results from the initial tests and the design of the final test matrix. Throughout the initial and final tests, the drop-mass was fixed at 55 lb. Additionally an $1/8^{th}$ inch thick piece of rubber was placed in the interface between the drop-mass and damper to avoid sensor ring due to metal-metal contact, Figure 4–1.

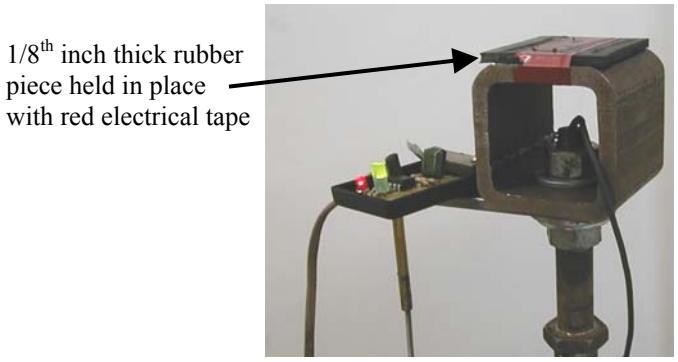

Figure 4–1. Rubber placed between drop-mass and damper to avoid sensor ring

4.1 Initial Test Matrix

The initial testing was conducted to ensure the sensors were properly functioning and to determine what type of other measurements may be necessary to classify the response of the fluid. Therefore, the tests were only performed once and repeatability was not investigated.

For the first round of testing, three drop-heights were selected: 24, 48 and 96 inches. These heights were selected to deliever a doubling in potential energy between each consecutive test and make use of the maximum drop-height available. To determine the effect of varying currents, five fixed currents were supplied to each damper for each drop-height as outlined in Table 4–1. The mono-tube MR damper received currents of 0, 1, 2, 4 and 5 A, and the double-ended MR damper was supplied with 0, 1, 2, 3 and 4 A. The currents were selected to capture the full range of possible currents to the MR

dampers. To power the MR dampers, the Protek 3005B DC Power Supply, Figure 4–2, supplied fixed DC current.

Figure 4–2. Protek 3005B DC Power Supply for providing current to MR dampers

The drop-mass acceleration, transmitted force and IR photogate signals were recorded simultaneously for each damper and each drop height. For the tests requiring power to the MR dampers, the current source was adjusted to the desired Amperage. Since MR dampers are designed to operate in the passive state and only require intermittent power to handle atypical loading, heating of the MR fluid and damper housing was avoided by releasing the drop-mass within one minute after powering the damper. In addition, during subsequent tests the dampers were given at least five minutes at the off state to avoid cumulative heating.

The first round of testing was conducted before the installation of the base-plate and piston accelerometers, and the LVDT. These sensors were determined to be necessary after analyzing the results from the initial tests, and were subsequently added to the experimental setup.

Table 4–1. Initial test matrix

MR Damper	Drop Height [in]	Impact Velocity [in/s]	Supply Current [A]
Mono-tube	24	127	0
			1
			2
			4
			5
	48	182	0
			1
			2
			4
			5
	96	260	0
			1
			2
			4
			5
Double-ended	24	127	0
			1
			2
			3
			4
	48	182	0
			1
			2
			3
			4
	96	260	0
			1
			2
			3
			4

4.2 Results from Initial Testing

After the initial testing was complete, the raw data was analyzed and preliminary conclusions were made. This section includes subsections on each of these topics.

4.2.1 Analysis of the Initial Test Results

To determine the point within the data sets where the impact began, the drop-mass accelerometer signal was used. Since the drop-mass went from +1 g to more than –50 g at the beginning of the impact, the start of the impact was determined by finding the first negative peak in the signal and then stepping backward through the data set until the acceleration of + 1 g was found. To check this method, the point where the IR flag circuit signal went low (right before the drop-mass and damper collided) was compared to the drop-mass acceleration calculation. These two beginning points typically agreed within less than 0.5 ms. However, since the drop-mass may rotate slightly as it is falling and may trigger the IR circuit before or after the true impact, the drop-mass acceleration calculation was used to mark the beginning of the impact event.

In addition to the beginning of the impact, a point to define the end of the impact was necessary. It was decided that the point defining the end of the impact was when the damper reached the point of maximum deflection. In other words, only the compression stroke of the damper was considered. Since the desired effect of a damper designed for an impact is to mitigate the impulse before bottoming out, it is sufficient to study just the compression stroke. To determine the end of the impact, the drop-mass acceleration signal was integrated once and the point when the velocity first crossed zero was considered the end of the impact. As will be discussed in Section 4.3, this method was inaccurate due to the rapid deceleration and another method was determined for the final tests.

For actually understanding what was going on with the fluid, the piston position and velocity were needed. Since there were no instruments directly mounted to the piston during the initial testing, the drop-mass was assumed to remain in contact and move as if rigidly attached to the piston from the beginning to the end of the impact. Under this assumption, the piston velocity and position were determined by integrating

the drop-mass accelerometer signal once and twice, respectively. This method was found inadequate, and an LVDT and piston accelerometer were added to the test set up for the final tests, as discussed in Section 4.3.

After the post processing was complete, plots of the drop mass acceleration and force transmitted to the base plate versus time were generated for each test. In addition, the force transmitted versus piston displacement and piston velocity were produced.

4.2.2 Conclusions from the initial testing

To summarize the results, the duration of the impact, the peak force transmitted to the base plate, maximum piston displacement and average load during the impact event were tabulated, Table 4–2. For a given drop height, as the supply current to the damper was increased the following trends were observed:

- Average force transmitted increases
- Displacement decreases
- Impact duration decreases

Since it has been extensively shown that increasing the supply current to an MR fluid increases the apparent yield stress of the fluid, these observations supported these findings. As the yield stress increases, the average force transmitted should increase and therefore the displacement should decrease. Furthermore, if the average force increases, the drop-mass would decelerate faster and the duration of the impact must decrease.

The fourth summary statistic, peak force transmitted, however, did not seem to follow any sort of trend with respect to supply current. This relationship is shown graphically for the mono-tube MR damper in Figure 4–3 and the double-ended MR damper in Figure 4–4. This presents a disagreement with the anticipated behavior of the MR fluid. Since the apparent yield stress increases with supply current, it was anticipated that the peak force transmitted would increase with supply current. However, the peak forces seem independent of the supply current. To account for this disagreement, it was hypothesized that the initial forces and high velocities associated with the impact will force the fluid into a region where the yield stress does not depend on the applied magnetic field. This result will be further discussed in Sections 5.1.3 and 6.1.3.

Table 4–2. Summary of results from initial testing

Damper	Drop Height (in) *Impact Velocity (in/s)*	Excitation (Amps)	Average Force Transmitted (lb)	Maximum Piston Displacement (in)	Impact Duration (ms)	Peak Force Transmitted (lb)
Mono-tube	24 *127*	0	557	2.66	38	1184
		1	561	2.29	34	1081
		2	558	2.46	35	1091
		4	624	2.40	33	1332
		5	645	1.91	29	1349
	48 *182*	0	885	2.40	31	2476
		1	830	2.61	33	2383
		2	950	2.22	29	2821
		4	1073	2.06	25	2596
		5	1217	1.96	23	2529
	96 *260*	0	1436	2.43	25	5444
		1	1512	2.36	23	7314
		2	1271	2.84	30	7348
		4	1495	2.59	24	7231
		5	1932	1.97	18	7182
Double-ended	24 *127*	0	298	3.87	72	2586
		1	308	2.87	73	2218
		2	448	2.34	49	2580
		3	590	1.94	38	2559
		4	677	1.77	33	2855
	48 *182*	0	531	4.51	57	4018
		1	450	2.88	61	4112
		2	558	3.23	54	4157
		3	664	2.94	45	4398
		4	792	2.35	36	4576
	96 *260*	0	818	3.82	39	6766
		1	870	5.39	45	6509
		2	780	4.48	50	6476
		3	744	5.05	53	6543
		4	829	4.70	50	6526

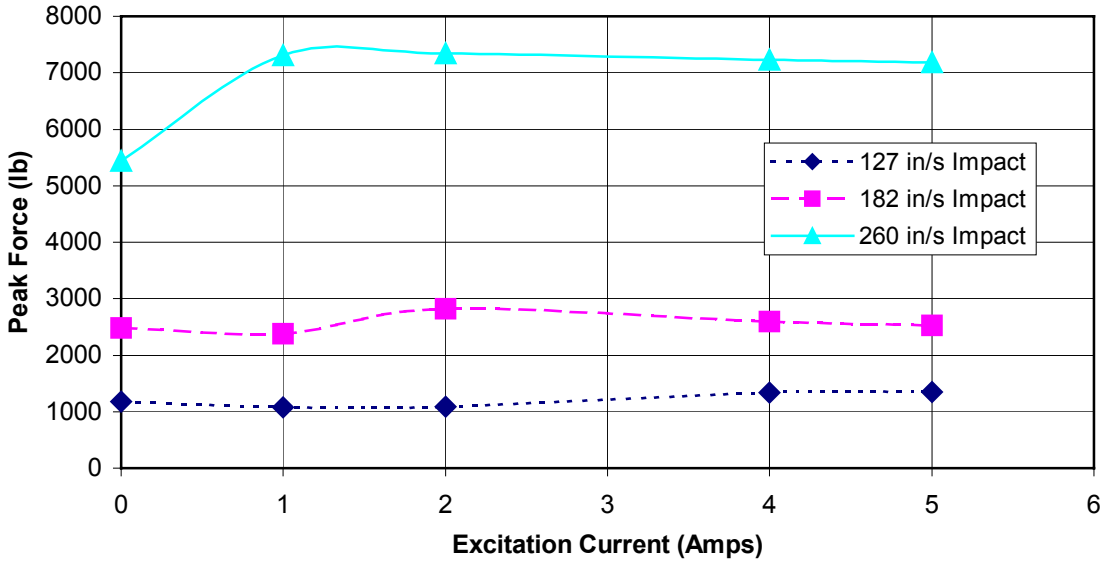

Figure 4–3. Peak force transmitted to the base plate for the mono-tube MR damper

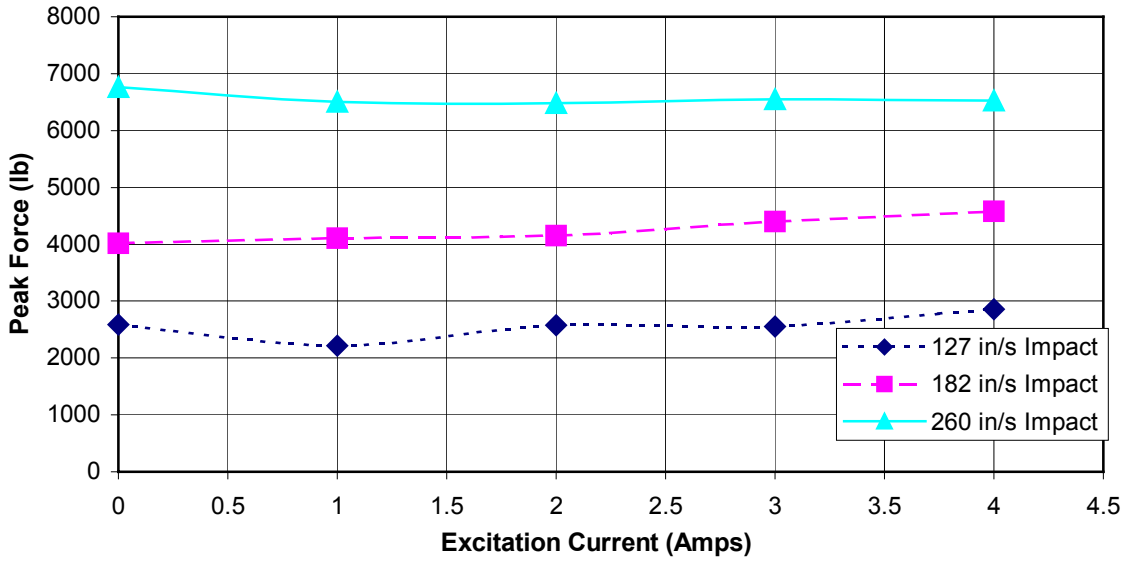

Figure 4–4. Peak force transmitted to the base plate for the double-ended MR damper

To further investigate the peak force transmitted, plots of the force transmitted versus piston displacement were generated. An interesting trend was observed in these plots. For the double-ended MR damper, the peak force occurred at the beginning of the stroke, while the peak force for the mono-tube damper tended to occur after midway

through the absorbed stroke. A representative plot of this relationship for the two dampers is presented in Figure 4–5. In order to clearly compare the two dampers, the force transmitted was normalized by the peak force and the displacement was normalized by the maximum displacement. It is important to note that for about the first 50% of the absorbed stroke, the mono-tube damper response resembles a spring. This characteristic was hypothesized to be due to the nitrogen accumulator and will be further discussed in Section 5.2.

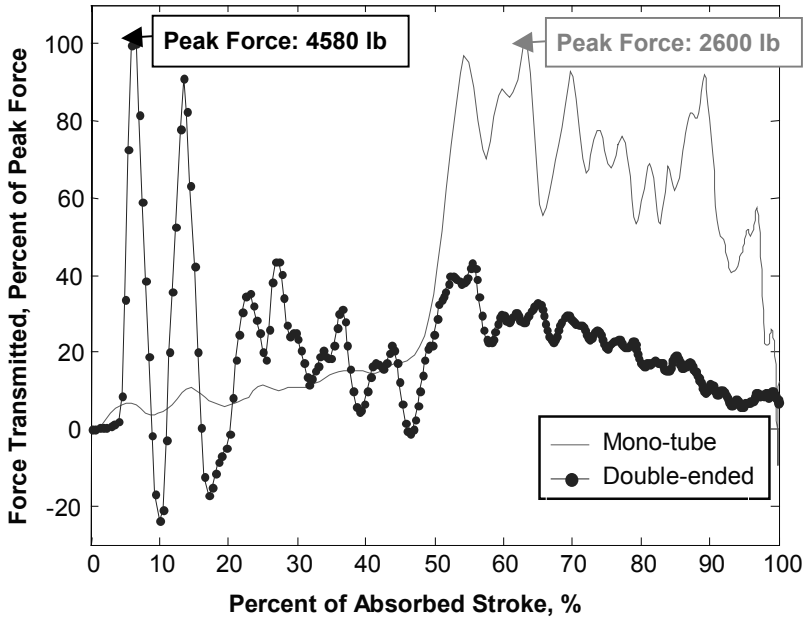

Figure 4–5. Force transmitted with respect to absorbed stroke for the two damper configurations*

*These two results are from a test with an impact velocity of 182 in/s and supply current of 4 Amps

4.3 Test Setup Modifications and Final Test Matrix

After analyzing the results from the initial tests, it was recognized that the piston acceleration, base plate acceleration and piston displacement should be directly monitored during the impact event. Additional improvements were necessary to the method for calculating the end of the impact and piston velocity. This section includes the reasons for the additional sensors and improved methods, and concludes with the development of the final test matrix.

4.3.1 Addition of Accelerometers and LVDT for Final Tests

Due to the high accelerations recorded for the drop-mass acceleration, it was hypothesized that it was insufficient to assume that the drop-mass and damper piston were moving in unison throughout the impact event. To describe the event more accurately, it was necessary to add an accelerometer to directly measure the piston acceleration for the final tests.

To further understand how the impact energy was being transmitted to the base-plate, an accelerometer was also fixed to the base-plate. The accelerometer was used to verify the behavior observed in the transmitted force data.

Since it was decided that the piston and drop-mass could not be approximated as rigidly attached, an LVDT was attached directly to the piston and the base-plate. The LVDT allowed for accurate measurement of the piston displacement relative to the piston housing.

The exact location, mounting method and specifications for these additional sensors are discussed in Section 3.3.1.

4.3.2 Modifications to Data Processing

For the initial tests, the end of the impact was determined by the point where the drop-mass velocity first crossed zero. However, since the drop-mass and piston were not moving in unison, this method did not accurately represent the ending point of the impact. With the addition of the LVDT, it was possible to determine the point where the piston completed the compression cycle. This point was used as the end of the impact event for the analysis of the final tests.

Since the noise associated with the LVDT was very low relative to the large change in output observed during compression, the piston velocity was determined directly from the LVDT data. The velocity, v_i, was calculated by taking the numerical derivative at each point, i, according to,

$$v_i = \frac{x_{i+1} - x_{i-1}}{t_{i+1} - t_{i-1}} \tag{4.1}$$

where x and t are the displacement data and time vector.

4.3.3 Development of the Final Test Matrix

From the initial tests, the peak force transmitted did not appear to depend on the excitation current. To verify this and other observed behaviors, it was decided that the final test matrix would be run three times. In addition, a lower drop height and a drop height halfway between the 48 and 96 inch drop heights were added to the test matrix. As shown in Table 4–3, the final test matrix included drop heights of 12, 24, 48, 72 and 96 inches and the five currents used in the initial testing.

Table 4–3. Final test matrix; Note: the entire test matrix was repeated three times

MR Damper	Drop Height [in]	Impact Velocity [in/s]	Supply Current [A]
Mono-tube	12	86	0, 1, 2, 4, 5
	24	127	0, 1, 2, 4, 5
	48	182	0, 1, 2, 4, 5
	72	224	0, 1, 2, 4, 5
	96	260	0, 1, 2, 4, 5
Double-ended	12	86	0, 1, 2, 3, 4
	24	127	0, 1, 2, 3, 4
	48	182	0, 1, 2, 3, 4
	72	224	0, 1, 2, 3, 4
	96	260	0, 1, 2, 3, 4

5 Analysis of the Mono-tube MR Damper Subject to Impulsive Loads

This chapter summarizes the data from the tests on the mono-tube MR damper. First, the general behavior of the damper is discussed and representative experimental plots are presented. Secondly, the observed behavior is divided up into two sections, the dynamics associated with the nitrogen accumulator and the dynamics associated with the MR fluid. Within each of these two sections, the experimental results and analytical justifications for the observed behavior are given. The chapter concludes with a section on characterizing the MR fluid flow.

5.1 Experimental Results from the Impulsive Tests

After reviewing the plots generated for the mono-tube MR damper, included in Appendix A, and compiling the statistics presented in Table 5–1, the following characteristics emerged:

- Average force transmitted to the base plate increased with increasing current
- Increasing the current results in a decrease in the amount of stroke used
- The peak force occurs after midway through the stroke and increasing the current does not affect the peak force transmitted for a given impact velocity
- The piston velocity curves were independent of current for all but the lowest impact velocity

This section is divided up into subsections that address the first three of these general characteristics and discuss possible reasons for the observed behavior. The forth observation is discussed in Section 5.3.

Table 5–1. Summary data for mono-tube MR damper (averages from three tests)

Drop Height (in) *Impact Velocity (in/s)*	Excitation (Amps)	Average Force Transmitted (lb)	Maximum Piston Displacement (in)	Impact Duration (ms)	Peak Force Transmitted (lb)
12 *86*	0	310	1.99	74	505
	1	292	1.89	60	502
	2	374	1.74	45	529
	4	469	1.48	36	657
	5	495	1.41	34	698
24 *127*	0	505	2.25	46	967
	1	511	2.23	45	992
	2	567	2.14	42	1049
	4	671	1.97	33	1145
	5	699	1.90	31	1231
48 *182*	0	703	2.52	41	2203
	1	709	2.43	40	2483
	2	765	2.41	38	2382
	4	884	2.28	31	2461
	5	931	2.20	30	2578
72 *224*	0	832	2.62	39	3548
	1	834	2.61	38	3557
	2	911	2.64	35	3024
	4	1013	2.50	30	3726
	5	1052	2.45	29	3772
96 *260*	0	988	2.79	37	5282
	1	967	2.75	37	5636
	2	1072	2.80	33	5034
	4	1237	2.69	29	5196
	5	1257	2.64	28	5251

5.1.1 Average Force Transmitted to the Base Plate

As shown in Figure 5–1, increasing the supply current to the mono-tube MR damper leads to an increase in the average force transmitted to the base-plate. Since previous work has shown that the apparent yield stress of the MR fluid increases with supply current, it follows that the average force transmitted should increase.

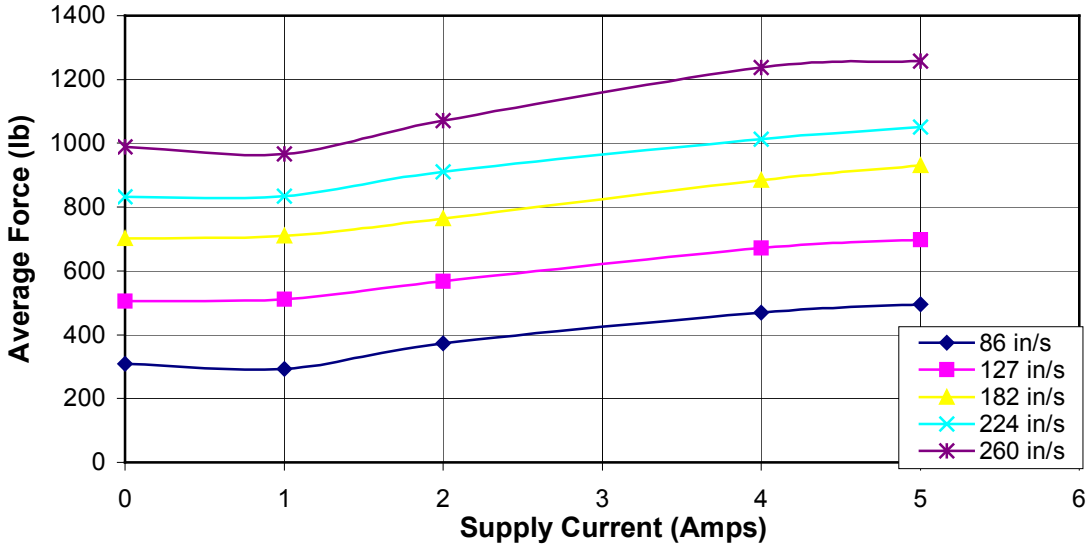

Figure 5–1. Average force transmitted versus current supplied for mono-tube MR damper

Also observed in Figure 5–1, the average force transmitted approximately doubles as the impact velocity doubles. Since a doubling in impact velocity is synonymous with a quadrupling in impact energy, to absorb this additional energy would require the stroke to double. However, by examining Table 5–1, it is clear that this is not always the case. The reason for this discrepancy is that the force measured on the base-plate is not the same as the force placed on the drop-mass by the damper piston. Wahed et al. have shown that the force input to the piston and force transmitted are not equivalent [5, 6].

5.1.2 Amount of Compression Stroke Used to Absorb Impulse

The maximum piston displacement tended to decrease with increasing current as shown in Figure 5–2. This trend agrees with the expected increase in apparent yield stress associated with increasing current. However, what is interesting in Figure 5–2 is the relative decrease in the piston displacement. For the highest impact velocity, the decrease between the maximum piston displacement from zero to 5 Amps is only 5 percent. While for the lowest impact velocity, the maximum piston displacement decreases 30% between the zero and full supply currents. Since the damper is not bottoming out, this trend implies that the higher impact velocities result in the fluid behaving independent of the supply current. This trend will be further discussed in relation to the controllability of the fluid in Sections 5.3 and 5.4.

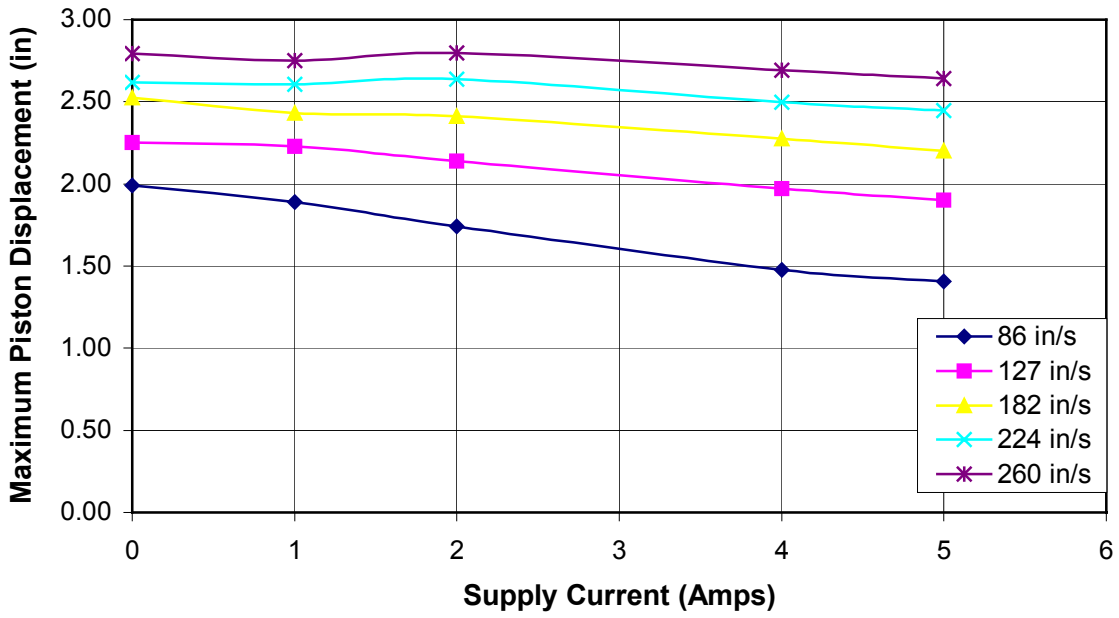

Figure 5–2. Maximum piston displacement versus supply current for varying impact velocities

5.1.3 Peak Force Transmitted to the Base Plate

The relationship between the peak force transmitted and the current supplied to the MR damper, Figure 5–3, does not exhibit any distinguishable trends with the exception of the lowest two impact velocities. As already discussed, it is hypothesized that the higher impact velocities force the fluid into a region where the behavior is independent of supply current. The independence of peak force and supply current disagrees with the results presented by Wahed et al. [5,6]. However, Wahed et al. investigated impact velocities and drop-masses that were orders of magnitude lower than those studied here and it is believed that they apparently did not encounter the behavior seen here. This relationship will be further discussed in Sections 5.3 and 5.4.

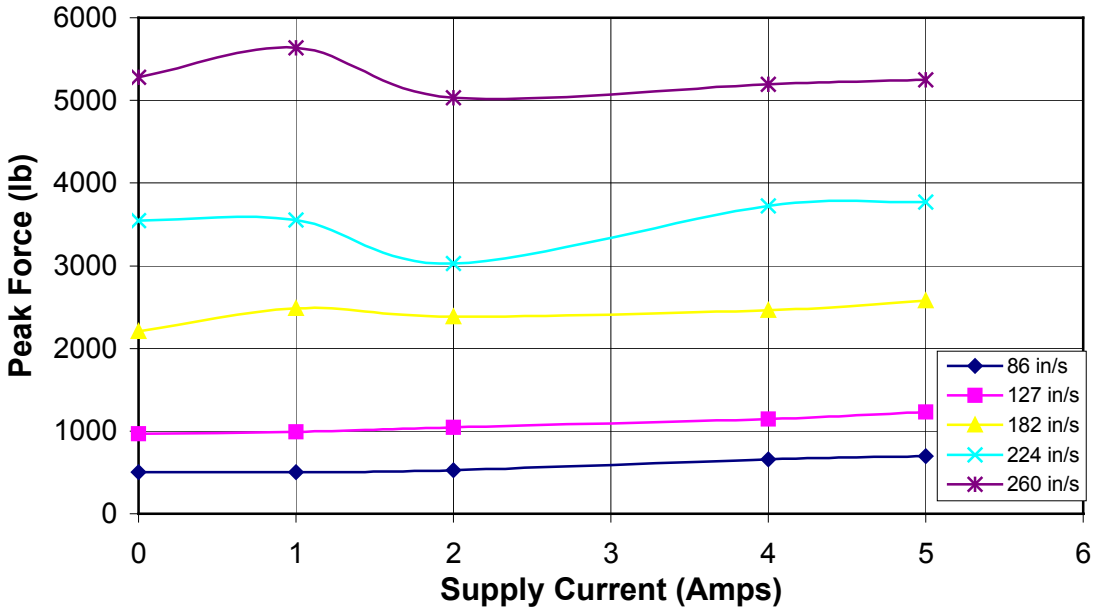

Figure 5–3. Peak force versus the supply current for varying impact velocities

5.2 Dynamics Associated with the Nitrogen Accumulator

The common technique for modeling the damping force produced by mono-tube MR dampers is to assume the damping force is dependent on only velocity and magnetic field strength. Under these assumptions, the dynamics of the accumulator are neglected. For low piston velocities this assumption has been well justified with experimental data [20].

For the mono-tube damper configuration studied, however, the sharp piston acceleration forces the fluid to behave almost as a solid for all but the lowest impact velocity. In other words, the fluid did not flow, or barely flowed, past the piston during the early stages of the impact. Thus, the damping provided by the flow of fluid through the gap is not taking place. Instead, the response of the accumulator dominates the characteristics of the "damping force." Damping force is in quotes because the force displacement data resembles a pre-loaded spring, as shown in the highlighted section of Figure 5–4.

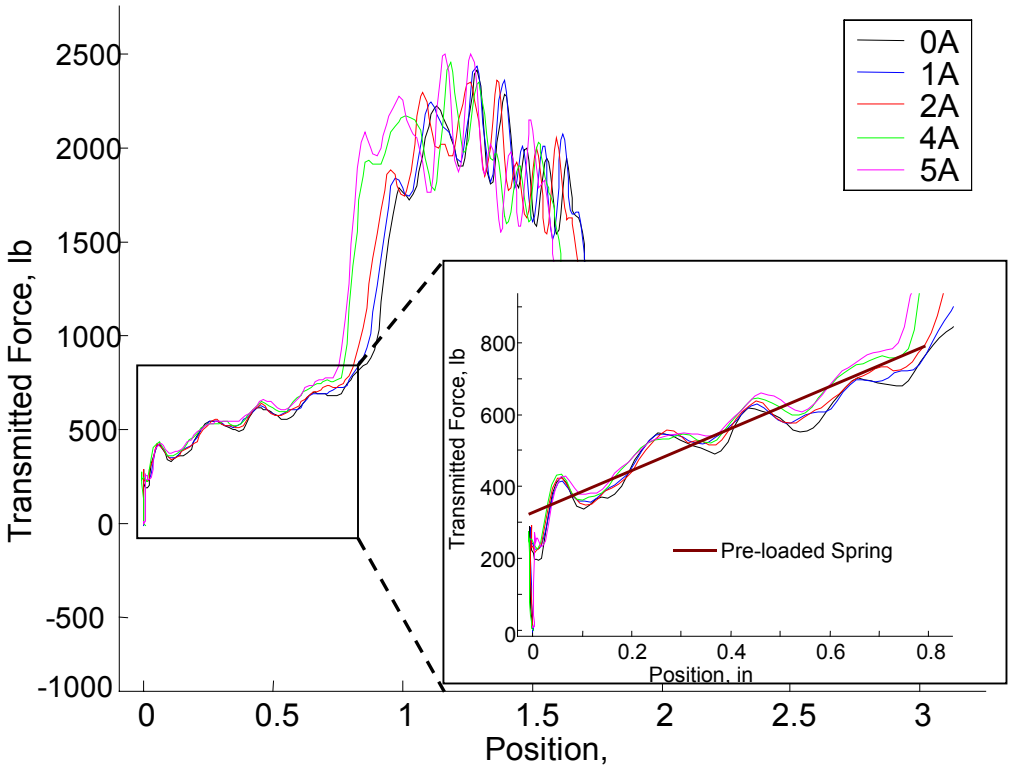

Figure 5–4. Force versus displacement graph for the mono-tube damper

To verify that this agreed with theory, the relationship between accumulator force and displacement was derived under the following assumptions:

- The compression of the nitrogen accumulator is isotropic, (T = constant)
- The temperature of the nitrogen was the same as the ambient conditions, in other words, tests were conducted far enough apart to avoid heating the nitrogen
- Nitrogen behaves as an ideal gas, $T/T_{cr} > 2$, (295 K/126 K = 2.34)
- The MR fluid does not flow until the accumulator bottoms out, therefore the accumulator piston displacement is equivalent with the piston displacement

The last assumption represents the most extreme case and in reality some of the fluid will flow through the gap. The variables defined for the derivation are graphically shown in Figure 5–5.

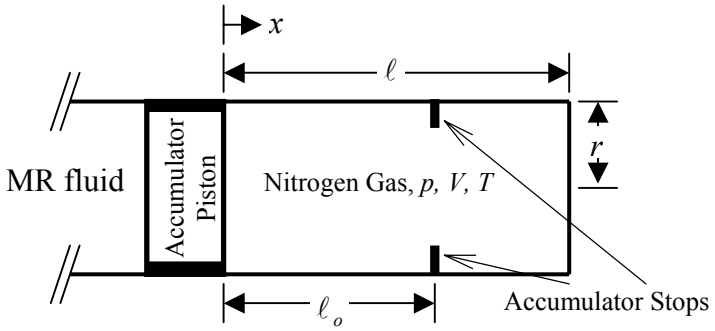

Figure 5–5. Nitrogen accumulator schematic for modeling

Since Nitrogen is assumed to behave as an ideal gas, the product of pressure, p, and volume, V, is a constant, C,

$$pV = C \tag{5.1}$$

Taking the derivative with respect to accumulator piston displacement, x, yields,

$$p\frac{dV}{dx} + V\frac{dp}{dx} = 0 \tag{5.2}$$

Recognizing $V(x) = \pi r^2(\ell - x)$, where r is the radius of the accumulator housing and ℓ is the equivalent length of the accumulator if it was a constant radius cylinder, and rearranging,

$$\frac{dp}{p} = \frac{\pi r^2}{\pi r^2 (\ell - x)} dx = \frac{1}{(\ell - x)} dx \tag{5.3}$$

Integrating from the initial pressure, p_o, and initial displacement, $x_o = 0$, to an arbitrary pressure, p, and displacement, x, yields,

$$\int_{p_o}^{p} \frac{dp}{p} = \int_0^x \frac{1}{(\ell - x)} dx$$

$$\ln(p) - \ln(p_o) = -\ln(\ell - x) + \ln(\ell) \tag{5.4}$$

$$\ln\left(\frac{p}{p_o}\right) = \ln\left(\frac{\ell}{\ell - x}\right)$$

Thus, provided the accumulator piston has not reached the stops ($x \le \ell_o$),

$$p(x) = p_o \left(\frac{1}{1 - \frac{x}{\ell}} \right) \tag{5.5}$$

By multiplying the pressure in the accumulator by the cross-sectional area perpendicular to the piston axis, the force produced by the accumulator, F, is,

$$F(x) = Ap(x) = \frac{\pi r^2 p_o}{1 - \frac{x}{\ell}}, \text{ where } x \le \ell_o \tag{5.6}$$

Once the accumulator piston reaches the stops, the contribution of the accumulator force to the "damping force" will be constant until the pressure exerted by the MR fluid on the accumulator is reduced to below this maximum pressure, $p(\ell_o)$.

For the MR damper tested, the accumulator properties are given in Table 5–2. Using the given properties, the relationship presented in Equation (5.6) was plotted over the force-displacement graphs (refer to Appendix A). A representative of these graphs, a test case of 182 in/s impact velocity, is shown in Figure 5–6. At the very beginning of the stroke, the accumulator force and force transmitted agree very closely. However, as the stroke continues to increase, the difference between the theoretical accumulator force

and the experimental force increases as shown in Figure 5–7(a). Since the velocity versus the stroke, shown in Figure 5–7(b), remains relatively constant after an initial acceleration, the increase in transmitted force above the theoretical accumulator force is hypothesized to be the result of an increase in the volume of fluid undergoing shear. This hypothesis is supported by the increasing difference as supply current is increased, which is related to the yield stress. Since the yield stress increases, the forces associated with shearing a given volume of fluid would increase.

In addition, the point where the accumulator bottoms out, marked be a sharp increase in the force transmitted, occurs earlier in the stroke for increased supply current. Because the yield stress is higher for increased currents, less fluid will flow through the gap, and the accumulator piston will bottom out earlier relative to the piston displacement. In other words, as the yield stress becomes greater, the assumption that the accumulator piston moves at the same rate as the damper piston is more valid.

Table 5–2. Accumulator properties of the mono-tube MR damper

Parameter	Value	Parameter	Value
Initial pressure, p_o	200 psia	Accumulator housing radius, r	0.6875 in
Initial volume, V_o	2.365 in^3	Maximum accumulator stroke, ℓ_o	0.95 in
Initial temperature, T	295 K	Equivalent cylinder length, ℓ	1.593 in

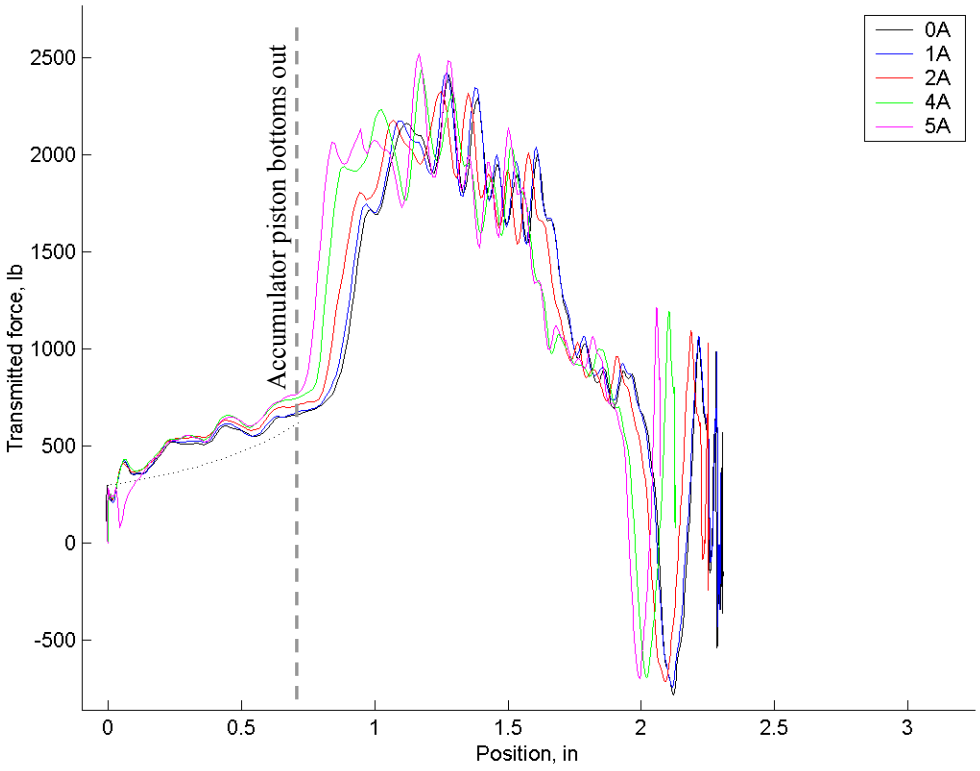

Figure 5–6. Comparison of theoretical force-displacement characteristic and experimental results

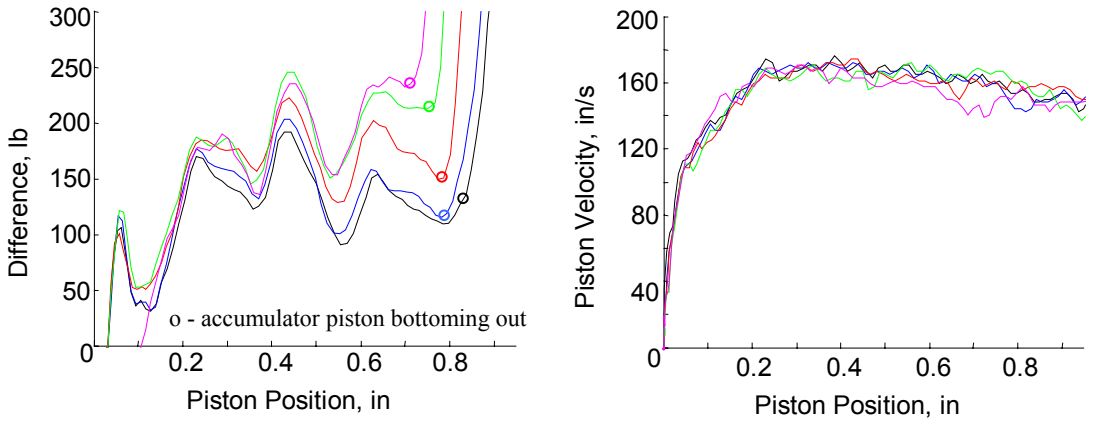

(a) **(b)**

Figure 5–7. Difference between accumulator model and experimental results (a) and corresponding piston velocity (b)

5.3 Dynamics Associated with the MR Fluid

For all but the lowest impact velocity, prior to the end of the accumulator piston stroke, the fluid in the gap is not flowing fast enough to account for the change in volume due to the piston displacement. As discussed in Section 5.2, by assuming the fluid is not flowing at all, the first part of the force displacement curve is accurately represented. Therefore, once the accumulator piston reaches the maximum stroke, the fluid is forced to flow through the gap to allow for any additional piston displacement. This is marked by a sharp increase in the force transmitted to the base as shown in Figure 5–8. The sharp increase in force is hypothesized to be due to the force required to drive the fluid through the gap.

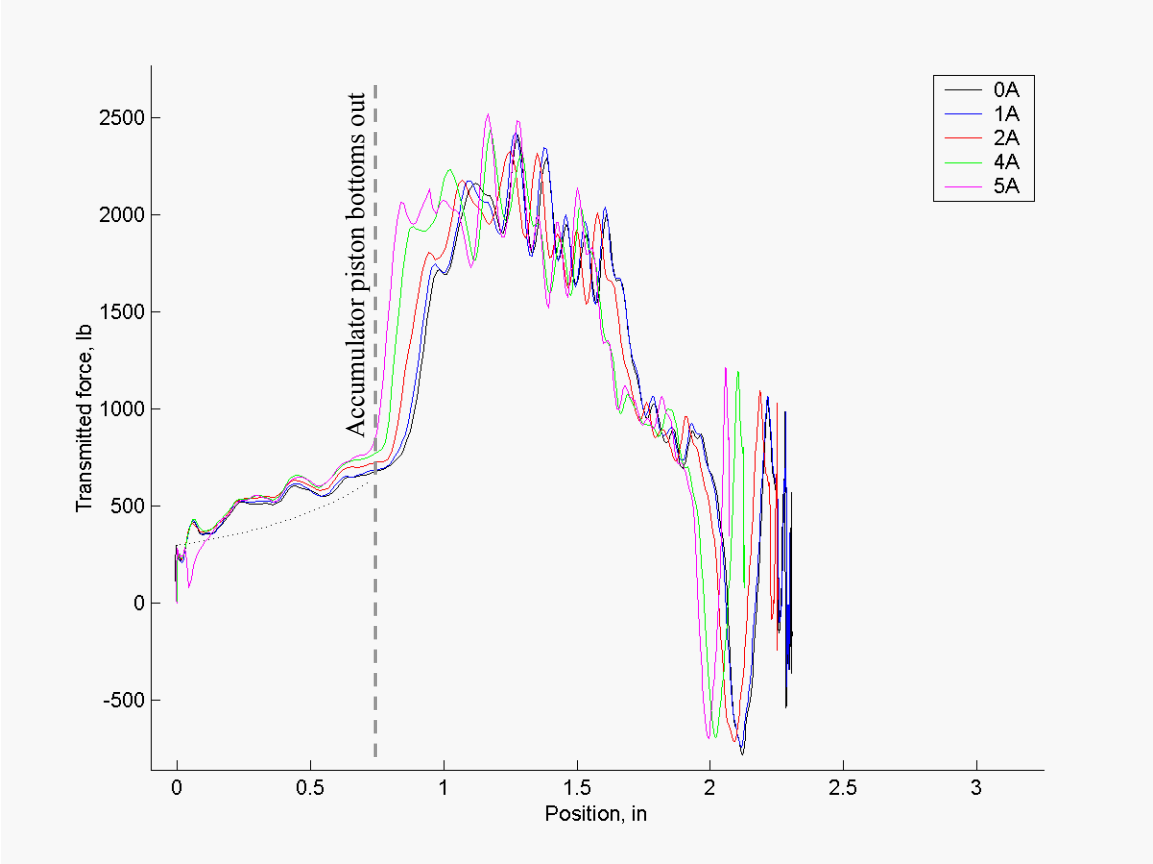

Figure 5–8. Force versus displacement for mono-tube MR damper

In examining the velocity versus time graphs, it appears that the piston velocity profiles were indistinguishable between varying currents for all but the lowest impact velocity. The lowest impact velocity differed in two important ways from the other impact velocities. First, modeling the beginning of the force displacement curve as an accumulator did not appear to fit, and second, for piston velocities under 45 in/s, the rate of piston deceleration was greater for increased currents, Figure 5–9. Since the damper piston mass, drop-mass and fluid are the same for each test, a difference in the rate of deceleration in the piston velocity must be related to the average force produced by the MR damper. It is important to point out that the force transmitted to the base plate also begins to vary with current at about the same point, however, it was easier to use the piston velocity graphs. Since the supply current is provided to the MR damper well before the impact event occurs, this behavior indicates that the damping force is not controllable except for when the damper piston velocity falls below 82 in/s.

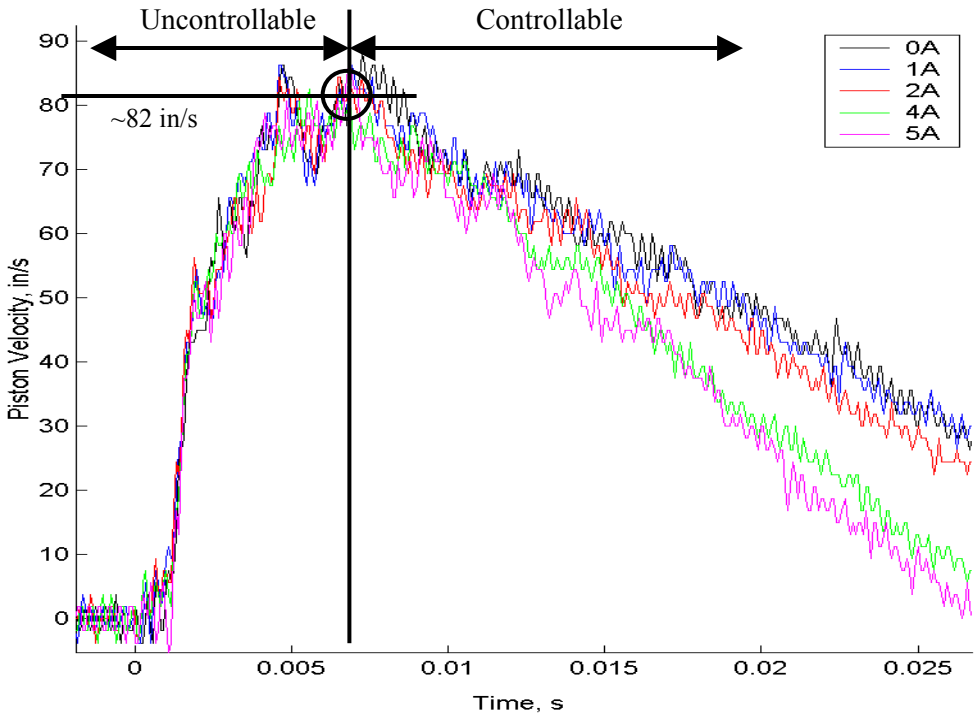

Figure 5–9. Piston velocity for lowest impact velocity (7 ft/s)

5.4 Characterization of MR Fluid Flow

To attempt to understand the point where the fluid becomes controllable at the lowest impact velocity, the Reynolds number was computed. The following assumptions were made:

- The MR fluid is incompressible
- No cavitation or vaporization are occurring when the fluid becomes controllable

It is important to restate that at the lowest impact velocity, the model of the accumulator force does not predict the force-displacement data. Therefore, the second assumption is valid and the MR fluid is hypothesized to be flowing fast enough to account for the piston displacement. Thus, the volume displaced by the piston must equate to the volume flowing through the annular gap. The relationship between the change in volume, *dV/dt*, piston velocity, v_{piston}, and the average fluid velocity through the gap, $\bar{v}$, may be written,

$$\begin{aligned} \frac{dV}{dt} &= \pi\left(r_{piston}^2 - r_{rod}^2\right)v_{piston} \\ &= \pi\left((r_{piston}+t)^2 - r_{piston}^2\right)\bar{v} \end{aligned} \tag{5.7}$$

where r_{piston} is the radius of the piston, r_{rod} is the radius of the piston rod and t is the gap thickness measured in the radial direction. Rearranging Equation (5.7), yields the relationship between the average velocity through the gap and the piston velocity,

$$\begin{aligned} \bar{v} &= \left(\frac{r_{piston}^2 - r_{rod}^2}{2r_{piston}t + t^2}\right)v_{piston} \\ &= \left(\frac{1-\left(\frac{r_{rod}}{r_{piston}}\right)^2}{2\left(\frac{t}{r_{piston}}\right)+\left(\frac{t}{r_{piston}}\right)^2}\right)v_{piston} \end{aligned} \tag{5.8}$$

For the dimensions of the mono-tube damper, the average fluid velocity through the gap is,

$$\bar{v} = 17.36 v_{piston} \tag{5.9}$$

Since the annular gap thickness is much smaller than the radius, the region between the piston and housing is approximated by infinite parallel plates. In addition, since the average fluid velocity is more than seventeen times the piston velocity, both plates will be considered stationary. Under these assumptions, the Reynolds number is given by,

$$\mathrm{Re} = \frac{\rho \bar{v} t}{\mu} \tag{5.10}$$

where ρ is the fluid density, t is the vertical separation between the two walls and μ is the viscosity of the fluid. The density and viscosity of the MR fluid used in the mono-tube MR damper are 3090 kg/m^3 and 0.09 Pa-s. Using Equations (5.9) and (5.10), the Reynolds number for the transition from uncontrollable to controllable, Re_T, was calculated to be,

$$\mathrm{Re}_T = \frac{\left(3090\,{}^{\mathrm{kg}}\!/_{\mathrm{m}^3}\right)\left(35.6\,{}^{\mathrm{m}}\!/_{\mathrm{s}}\right)\left(3.81\times10^{-4}\ \mathrm{m}\right)}{0.09\,\mathrm{Pa}\cdot\mathrm{s}} \approx 466 \tag{5.11}$$

Note that the piston velocity for the calculation of the Re_T was 82 in/s, which leads to an average fluid velocity of 1424 in/s or 35.6 m/s.

For flow through infinite parallel plates, transition from laminar to turbulent occurs roughly around a Reynolds number of 2000. It was initially hypothesized that the point where the fluid transitions from controllable to uncontrollable might be explained by the transition from laminar to turbulent. However, since the point when the fluid becomes controllable is well below the conditions for turbulent flow and this behavior was only observed for the lowest impact velocity, other factors must be involved. For instance, it is possible that the fluid is undergoing a phase change due to the extremely high fluid velocities. Investigating this relationship is beyond the scope of the current work, but presents a very interesting topic for future research.

6 Analysis of the Double-Ended MR Damper Subject to Impulsive Loads

This chapter summarizes the data from the tests on the double-ended MR damper. First, the general behavior of the damper is discussed, representative experimental plots are presented and possible reasons for the observed behavior are given. Secondly, the dynamics of the MR fluid flow are characterized.

6.1 Experimental Results from Impulsive Tests

After reviewing the plots generated for the double-ended MR damper, included in Appendix B, and compiling the statistics presented in Table 6–1, the following characteristics emerged:

- Average force transmitted to the base plate only exhibited trends for the 86 and 127 in/s impact velocities
- Increasing the current results in a decrease in the amount of stroke used
- The peak force occurs at the beginning of stroke and increasing the current does not affect the peak force transmitted
- For a given impact velocity, the piston velocity was independent of current until the piston velocity decreased below roughly 100 in/s

This section is divided into subsections that address these general characteristics and discuss possible reasons for the observed behavior.

Table 6–1. Summary data for double-ended MR damper (averages from three tests)

Drop Height (in) *Impact Velocity (in/s)*	Excitation (Amps)	Average Force Transmitted (lb)	Maximum Piston Displacement (in)	Impact Duration (ms)	Peak Force Transmitted (lb)
12 *86*	0	208	4.38	98	1904
	1	217	2.69	92	1557
	2	361	1.51	46	1614
	3	476	1.12	34	1629
	4	544	0.97	28	1745
24 *127*	0	364	4.39	81	2550
	1	268	3.83	103	2604
	2	427	2.39	56	2676
	3	546	1.90	42	2817
	4	626	1.68	36	2844
48 *182*	0	551	4.38	61	4168
	1	468	4.37	67	4133
	2	499	3.42	61	4417
	3	616	2.87	49	4508
	4	684	2.61	44	4531
72 *224*	0	682	4.39	50	5283
	1	626	4.37	52	5387
	2	541	4.07	63	5571
	3	613	3.57	54	5205
	4	704	3.27	47	5488
96 *260*	0	858	4.38	44	5846
	1	797	4.37	45	5922
	2	737	4.34	51	6169
	3	703	3.99	54	6234
	4	749	3.72	48	6283

6.1.1 Average Force Transmitted to the Base Plate

For the two lowest impact velocities, 86 and 127 in/s, the average force transmitted to the base plate increased with increasing current, as shown in Figure 6–1. The reason that the supply current of zero Amps tends to yield higher average forces is due to the presence of high forces when the damper bottoms out, which were included in the average force calculations. For the other three impact velocities, it was not possible to discern a relationship. Since previous work has shown that the yield stress of the MR fluid increases with supply current, it follows that the average force transmitted should increase. The disagreement of the higher impact velocities is attributed to the higher velocities forcing the fluid into a regime that does not depend on supply current for a significant portion of the stroke. This result will be further discussed in Section 6.2.

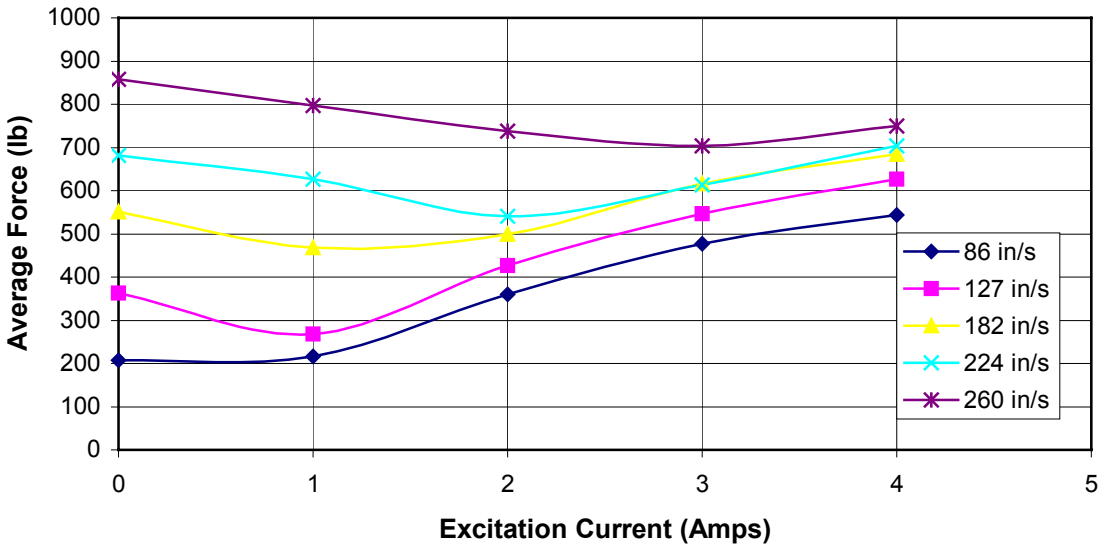

Figure 6–1. Average force transmitted versus current supplied for double-ended MR damper

6.1.2 Amount of Compression Stroke Used to Absorb Impulse

The maximum piston displacement for the double-ended damper tends to decrease with increasing supply current, Figure 6–2. This result agrees with the notion that increasing supply current increases the apparent yield stress of the fluid. For a given supply current, it is also clear that increasing the impact velocity causes addition stroke to be used in absorbing the impact. Although it would be logical to calculate the average force from the amount of stroke used and the change in kinetic energy during the impact, this was not possible because the drop-mass often bounced after the maximum stroke was reached.

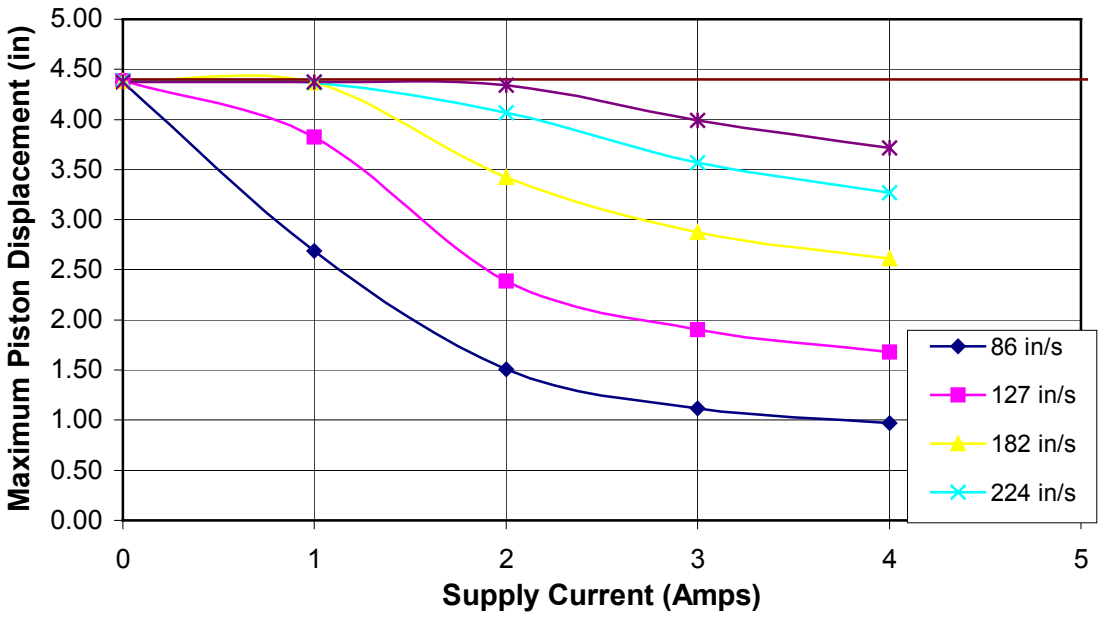

Figure 6–2. Maximum piston displacement versus supply current for varied impact velocities

6.1.3 Peak Force Transmitted to the Base Plate

The peak force transmitted to the base plate remained nearly constant for varying currents, as shown in Figure 6–3. Since the peak force occurred at the beginning of the stroke, it is hypothesized that the initial impact forces the fluid to respond independent of supply current. As mentioned for the mono-tube case, Section 5.1.3, this result does not agree with the results presented by Wahed et al. [5,6]. Wahed et al. found that increasing the supply to the MR damper resulted in increases in the peak force transmitted. The disagreement is attributed to the greater impact velocities and drop-mass used in this study.

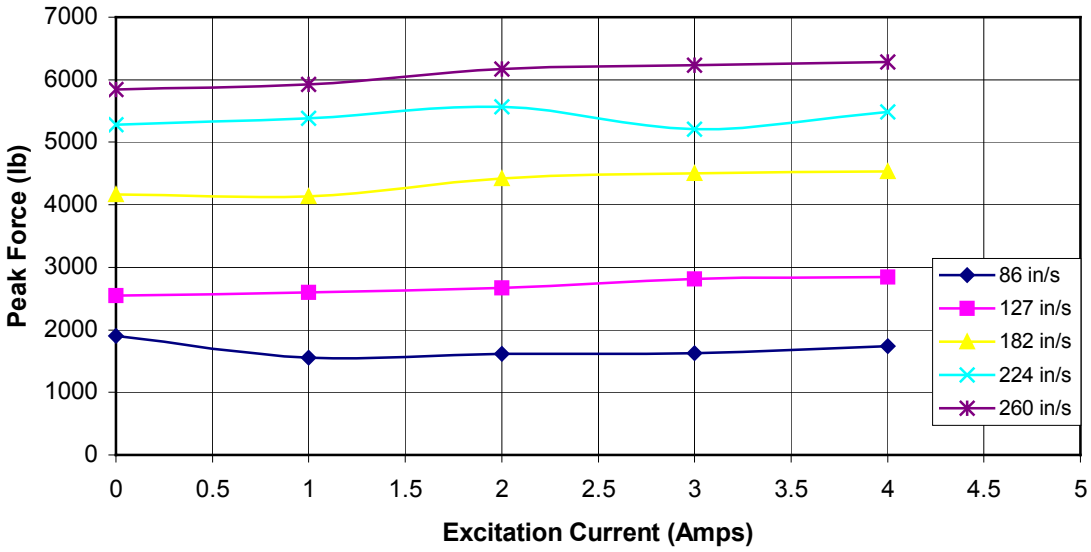

Figure 6–3. Peak force transmitted versus supply current for double-ended MR damper*

*Each point represents an average from three tests

6.1.4 Piston Velocity

During the initial impulse, piston velocities appear to follow each other very closely for a given impact velocity. However, once the piston velocity dropped below some threshold, the average deceleration increased for increasing supply current. An example of this behavior is shown in Figure 6–4.

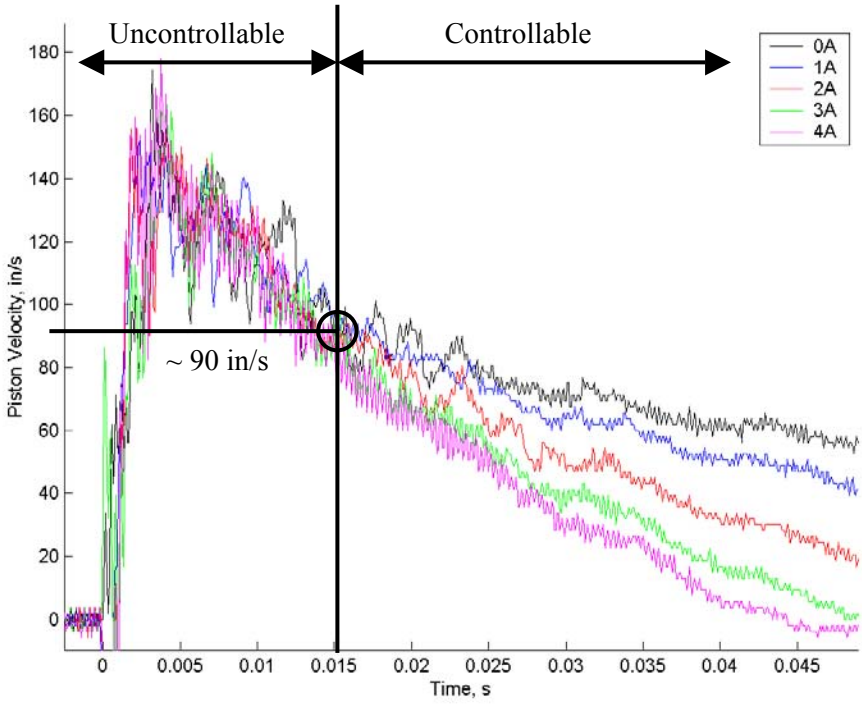

Figure 6–4. Representative graph of piston velocity, the circle marks the threshold piston velocity

Since the damper piston mass, drop-mass and fluid are the same for each test, the rate of acceleration/deceleration must be related to the average force produced by the MR damper. Prior to the threshold velocity, the piston velocity follows a very similar trend and it is not possible to distinguish between the piston velocities based on the supply current. Therefore, the initial impact forces result in MR fluid behavior that does not depend on the supply current. Since the supply current is provided to the MR damper well before the impact event occurs, this behavior indicates that the damping force is not controllable above the threshold velocity. It is important to point out that the force transmitted to the base plate varies with current after the velocity falls below the

threshold velocity as well, however, it was easier to use the piston velocity graphs to determine the threshold velocity.

The average of these threshold values for each of the impact velocities is summarized in Table 6–2. The threshold values are lower for the slower impact velocities.

Table 6–2. Average threshold piston velocity

Impact velocity [in/s]	Piston velocity [in/s]*
86	65
127	90
182	100
224	105
260	115

6.2 Characterization of the MR Fluid Flow

In an attempt to understand why the damping force is independent of the supply current during the initial part of the impact event, the Reynolds number at the threshold velocity is derived. For this calculation, the following assumptions were made:

- The MR fluid is incompressible
- The piston and piston rods do not deform during the impact event
- The MR fluid is not undergoing cavitation or vaporization

Under these assumptions, the volume displaced by the piston must equate to the volume flowing through the annular gap. Therefore, the relationship between the change in volume, dV/dt, piston velocity, v_{piston}, and the average fluid velocity through the gap, $\bar{v}$, may be written,

$$\begin{aligned} \frac{dV}{dt} &= \pi\left(r_{piston}^2 - r_{rod}^2\right)v_{piston} \\ &= \pi\left((r_{piston}+t)^2 - r_{piston}^2\right)\bar{v} \end{aligned} \tag{6.1}$$

where r_{piston} is the radius of the piston, r_{rod} is the radius of the piston rod and t is the gap thickness measured in the radial direction. Rearranging Equation (6.1), yields the relationship between the average velocity through the gap and the piston velocity,

$$\begin{aligned}\bar{v} &= \left(\frac{r_{piston}^2 - r_{rod}^2}{2r_{piston}t + t^2}\right)v_{piston} \\ &= \left(\frac{1-\left(\frac{r_{rod}}{r_{piston}}\right)^2}{2\left(\frac{t}{r_{piston}}\right)+\left(\frac{t}{r_{piston}}\right)^2}\right)v_{piston}\end{aligned} \tag{6.2}$$

For the dimensions of the double-ended damper, the average fluid velocity through the gap is,

$$\bar{v} = 5.358 v_{piston} \tag{6.3}$$

Since the annular gap thickness is much smaller than the radius, the region between the piston and housing is approximated by infinite parallel plates. In addition, since the average fluid velocity is more than five times the piston velocity, both plates will be considered stationary. Under these assumptions, the Reynolds number is given by,

$$\mathrm{Re} = \frac{\rho \bar{v} t}{\mu} \tag{6.4}$$

where ρ is the fluid density, t is the vertical separation between the two walls and μ is the viscosity of the fluid. The density and viscosity of the MR fluid used in the double-ended MR damper are 3090 kg/m^3 and 0.09 Pa-s, respectively. Using Equations (6.3) and (6.4), the Reynolds numbers for the threshold, Re_T, and maximum, Re_{max}, fluid velocities were calculated and compiled in Table 6–3. The threshold Reynolds numbers are around the value associated with transition from laminar to turbulent flow. As such, it is hypothesized that the transition from uncontrollable to controllable is related to the transition from turbulent to laminar.

Table 6–3. Reynolds numbers at maximum and threshold fluid velocities

Impact velocity [in/s]	Maximum fluid velocity [in/s]*	Re_{max}	Threshold fluid velocity [in/s]*	Re_T
86	510	1300	360	920
127	630	1600	480	1200
182	890	2300	560	1400
224	1070	2700	580	1500
260	1290	3300	610	1600

*Note: These fluid velocities are the average of the fluid traveling through the gap for the maximum and threshold flow rates

By plotting the threshold and maximum Reynolds numbers versus the impact velocity, it appears that the threshold Reynolds number is approaching an upper limit, Figure 6–5. In other words, as the impact velocity is increased the fluid reaches a point where it will only be controllable for Reynolds numbers less than 1600. It is important to keep in mind that the drop-mass was constant throughout this study, and it is hypothesized that changing the drop-mass may affect these trends as well. However, investigating this relationship is beyond the scope of this work.

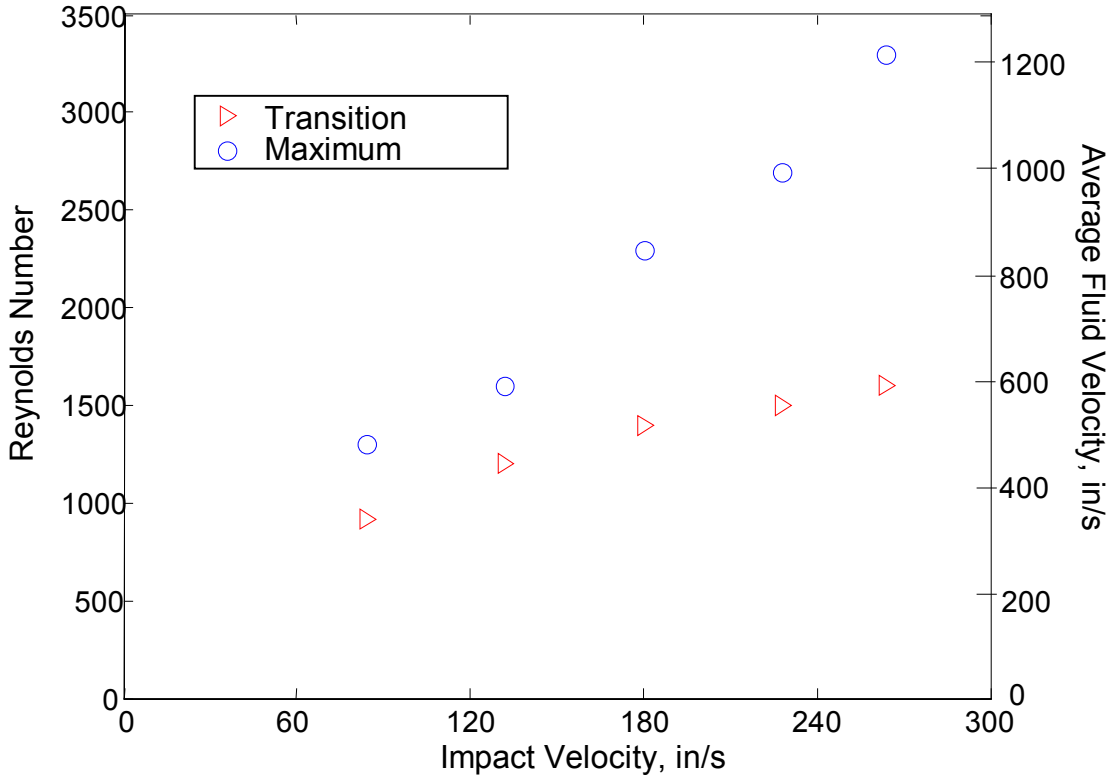

Figure 6–5. Reynolds number versus the impact velocity

7 Comparison of the Mono-Tube and Double-Ended MR Damper Designs for Mitigating Impulsive Loads

In reviewing the results from the two MR damper configurations, there were a number of differences between the characteristics of their responses. This chapter highlights these differences and discusses the advantage/disadvantage of each for mitigating impact excitations.

7.1 Peak Force Transmitted

Since the mono-tube and double-ended MR damper magnetic circuit constructions are very different, it is not possible to compare the peak force transmitted for any of the tests where power was supplied to the MR dampers. However, it is possible to compare the two dampers when no current was supplied.

For any given impact velocity and zero supply current, the peak of the force transmitted to the base plate was lower for the mono-tube MR damper. This result was not expected. Because the annular gap for the double-ended design is an order of magnitude larger than the gap in the mono-tube design (0.115 in >> 0.015 in), it was hypothesized that the double-ended design would allow more fluid flow and a lower peak force would be transmitted. As discussed earlier, the nitrogen accumulator governs the initial behavior of the mono-tube design and the peak force does not occur until midway through the stroke. Thus, it is hypothesized that the peak force is lower for the mono-tube design because by the time the fluid is forced to flow, the accumulator has absorbed a significant amount of the initial impact energy.

With regards to the peak force transmitted, the mono-tube design offers an advantage over the double-ended design. However, as will be discussed in the next section, for the majority of the stroke the damping forces for the mono-tube design are not controllable.

7.2 Controllability During Impulsive Event

As defined in Sections 5.4 and 6.2, a MR damper subject to an impact was uncontrollable until it was clear that the piston deceleration depended on supply current. To better

compare the usefulness of a MR damper during an impulsive event, the percent of controllable stroke, $S_{percent}$, is defined as,

$$S_{percent} = \frac{S_{control}}{S_{\max}} \cdot 100$$

where $S_{control}$ is the amount of stroke from the transition point to the maximum stroke at zero supply current and S_{max} is the maximum stroke used at zero supply current.

In the case of the mono-tube MR damper, the percent of controllable stroke was 60% at the lowest impact velocity. For all of the other impact velocities, the mono-tube MR damper was not controllable. The percent of controllable stroke was tabulated for both MR dampers in Table 7–1.

Table 7–1. Comparison of percent of controllable stroke

Impact velocity [in/s]	Percent of controllable stroke	
	Mono-tube Damper	Double-ended Damper
86	60	90
127	0	80
182	0	65
224	0	50
260	0	45

By examining Table 7–1, it is clear that the damping forces of the double-ended MR damper are controllable for a much larger percent of the stroke. It is hypothesized that the larger gap size of the double-ended MR damper and lack of an accumulator are responsible for this trend. The absence of the accumulator requires the fluid to flow from the initial point of impact and the larger gap size equates to lower average flow rates through the gap.

8 Conclusions and Recommendations

This chapter is divided into two sections. The first section summarizes the results of the research performed for the thesis. The second section presents recommendations for future work for understanding the behavior of magnetorheological fluids subject to impact behavior.

8.1 Summary

Three primary objectives were outlined in Chapter 1. The objectives included: (1) developing a drop-tower testing facility; (2) evaluating the behavior of magnetorheological fluids during impulsive excitation; and (3) providing a basic understanding of how MR damper device design relates to the ability to handle inputs that result in high velocities. This section discusses how each objective was met and a brief synopsis of the results.

The first objective was to develop a drop-tower test facility that would provide impact excitation to the MR dampers. The drop-tower test facility designed and constructed included a drop-mass that may be varied from 55 to 500 lbs. Due to the scope of this study, the nominal drop-mass of 55 lbs was used throughout. The drop-tower test facility allows the drop-mass to be released at any height between 0 and 100 inches. In addition, the drop-tower facility was instrumented to monitor the response of the MR damper to impulsive excitation. After an initial round of testing, additional sensors to monitor the impact event were incorporated into the design. The final list of sensors included:

- Three accelerometers, mounted to the base-plate, piston and drop-mass to monitor the respective accelerations
- An LVDT mounted to the piston, to measure the piston displacement
- Three load cells under the base-plate to monitor the force transmitted
- An infrared circuit to determine the impact velocity

A data acquisition system and computer were set up to record the signals and methods were developed to process the raw data signals.

The second objective was to evaluate the behavior of magnetorheological fluids during impulsive excitation. By subjecting the two MR damper configurations to varying impulsive loads and varying the supply current, the response of the MR fluid was studied.

The mono-tube MR damper exhibited a response that was governed by the dynamics of the accumulator for the first part of the stroke. As such, it was determined that the MR fluid was not flowing fast enough to accommodate the rapid piston displacement. Once the accumulator bottomed out, the MR fluid was forced to flow and the damping force increased by an order of magnitude.

For all but the lowest impact velocity, the velocity profiles did not depend on the supply current, and it was hypothesized that the MR fluid was not controllable for these cases. At the lowest impact velocity, the MR fluid only became what was defined as controllable once the piston velocity fell below about 82 in/s. To explain this transition, the Reynolds number was calculated at this piston velocity. However, the Reynolds number was significantly below the common Reynolds number for transition from turbulent to laminar. A number of possible explanations were suggested, including that the fluid may have been undergoing a phase change or that controllability is not related to the type of flow. Further research in this area will be necessary to determine the exact relationship between controllability and flow characteristics.

Upon impact, the double-ended MR damper transmitted the greatest force observed during the impact event. The large force transmitted was hypothesized to be the force required to accelerate the fluid. For all of the tests on the double-ended MR damper, the fluid became controllable once the piston velocity dropped below a threshold value. The relationship between the threshold value and fluid characteristics showed that the transition to controllable tended to occur at about the same point the flow was transitioning from turbulent to laminar.

The third objective was to provide a basic understanding of how MR damper device design relates to the ability to handle inputs that result in high velocities. As presented in Chapter 7, the two MR damper designs handle impulsive loads differently. The peak force transmitted by the mono-tube MR damper was significantly lower than the peak force transmitted by the double-ended MR damper. This reason the mono-tube MR damper transmitted a lower peak force was hypothesized to be the result of the

energy absorbed by the accumulator, which occurred before the MR fluid was forced to flow. However, for all but the lowest impact velocity, the mono-tube MR damper did not appear to exploit the properties of the MR fluid. In other words, the mono-tube MR damper was not controllable during the impact event. The amount of controllable stroke for each design was compiled and the double-ended MR damper proved to provide a much greater percentage of the stroke that could be used for controlling the impact event.

8.2 Recommendations for Future Research

During the analysis of the data, a number of possible extensions to further understand the behavior of magnetorheological fluids subject to impulsive loads were encountered. This section includes additional areas that could be explored with the current drop-tower test facility, as well as other areas that may be explored independent of the test facility.

8.2.1 Future Research with the Drop-Tower Test Facility

For future studies using the drop-tower test facility, it is suggested that a sensor to directly measure the force input to the piston be incorporated into the test set-up. If the input force was known, it would be possible to calculate the ratio of the force transmitted to the base-plate and also estimate the energy absorbed by the MR damper.

An extension of this work would be to study the relationship between the magnitude of the drop-mass and the dynamic response of the MR dampers. It is hypothesized that increasing the mass would be similar to increasing the drop height, since the amount of energy imparted to the damper is related to the product of mass and drop height.

8.2.2 Future Research on MR Fluid Behavior

As discussed in Section 5.2, the initial response of the mono-tube MR damper was governed by the dynamics of the accumulator. Additional modeling of the accumulator and MR fluid interaction may be used to develop an accumulator that does not bottom out. It is hypothesized that if the accumulator does not bottom out, the MR damper may be controllable for a greater percentage of the stroke.

Since the accumulator was not able to provide the pressure required to force the fluid to flow through the gap, another possible area of research would include developing a model that incorporates the fluid inertia effects. One of the first assumptions made by researchers modeling MR dampers is to neglect the fluid inertia effects. However, as shown in this study, during impulsive excitation, the inertia of the fluid plays a very important role in the dynamics of the response.

This work revealed that the fluid appears to become controllable once piston velocities slow below some threshold. It is suggested that this relationship be further explored by modeling the fluid, including inertia terms, and incorporating a model of the magnetic field as well.

References:

1. Ahmadian, M., Poynor, J. C., Gooch, J.M., "Application of Magneto Rheological Dampers for Controlling Shock Loading," *ASME Dynamics Systems & Control Division, DSC, Vol. 67*, p. 731-735, 1999.
2. Ahmadian, M., Appleton, R. and Norris J.
3. Ahmadian, M., Appleton, R. and Norris J.
4. Tanner, T., "Combined Shock and Vibration Isolation through the Self-Powered, Semi-Active Control of a Magnetorheological Fluid Damper in Parallel with an Air Spring," Summary of Research, Northup Grumman Newport News, December, 2002.
5. El Wahed, A. K., Sproston, J. L. and Schleyer, G. K., "Electrorheological and Magnetorheological Fluids in Blast Resistant Design Applications," *Materials and Design, Vol. 23,* No. 4, pp. 391-404, 2002.
6. El Wahed, A. K., Sproston, J. L. and Schleyer, G. K., "A Comparison Between Electrorheological and Magnetorheological Fluids Subjected to Impulsive Loads," *Proceedings of the Seventh International Conference on Electrorheological (ER) and Magnetorheological (MR) Suspensions,* 1998, pp. 401-410.
7. Phule, P., "Magnetorheological (MR) Fluids: Principles and Applications," *Smart Materials Bulletin, Vol. 2001,* Issue 2, pp. 7-10, February 2001.
8. Gavin, H., Hoagg, J., and Dobossy, M., "Optimal Design of MR Dampers," P*roceedings of U.S.-Japan Workshop on Smart Structures for Improved Seismic Performance in Urban Regions*, K. Kawashima, et al., eds., Seattle WA, pp. 225-236, 2001.
9. Poynor, J. C., *Innovative Designs for Magneto-Rheological Dampers*, M.S. thesis, Virginia Polytechnic Institute and State University, Blacksburg, VA, 2001.
10. QED Technologies web page, http://www.qedmrf.com
11. "MR Brake, MRB-2107-3", Lord Corporation product bulletin, Cary, NC, 2003.

12. Lindler, J. E., Dimock, G. A. and Wereley, N. M., "Design of a Magnetorheological Automotive Shock Absorber," *Proceedings of SPIE, Vol. 3985*, pp. 426-437, 2000.

13. Simon, D. E. and Ahmadian, M., "Application of Magneto-Rheological Dampers for Heavy Truck Suspensions," *Proceedings of the 32nd International Symposium on Automotive Technology and Automation (ISATA)*, Vienna, Austria, 1999.

14. Kelso, S. P., "Experimental Characterization of Commercially Practical Magnetorheological Fluid Damper Technology," *Proceedings of SPIE, Vol. 4332,* pp. 292- 299, 2001.

15. Dana Technology website, http://www.dana.com/technology/intelldriveshaft.shtm

16. Liu, J., Anthony, F. and Rongsheng, S., "In-vitro Investigation of Blood Embolization in Cancer Treatment Using Magnetorheological Fluids," *Journal of Magnetism and Magnetic Materials, Vol. 225*, pp. 209-217, 2001.

17. Carlson, J. D., Matthis, W., and Toscano, J. R., "Smart Prosthetics based on Magnetorheological Fluids," *SPIE 8th Annual Symposium on Smart Structures and Materials*, Newport Beach, CA, 2001.

18. Yang, G., Carlson, J.D., Sain, M.K., Spencer, B.F., "Large-scale MR fluid dampers: Modeling and dynamic performance considerations," *Engineering Structures, Vol. 24, No. 3*, p. 309-323, 2002.

19. Lord Corporation website, http://www.mrfluid.com

20. Snyder, R. A., Kamath, G. M., and Wereley, N. M., "Characterization and Analysis of Magnetorheological Damper Behavior Under Sinusoidal Loading," *AIAA Journal, Vol. 39,* No. 7, pp. 1240-1253, July 2001.

21. Stanway, R., Sproston, J. L., and El-Wahed, A. K., "Application of Electrorheological Fluids in Vibration Control: A Survey," *Smart Materials and Structures, Vol. 5, No. 4,* pp. 464-482, 1996.

22. Spencer Jr., B. F., Dyke, S. J., Sain, M. K., and Carlson, J. D., "Phenomenological Model of a Magnetorheological Damper," *Journal of Engineering Mechanics, ASCE*, *Vol. 123,* pp. 230-238, 1997.

23. Wang, X. and Gordaninejad, F., "Dynamic Modeling of Semi-Active ER/MR Fluid Dampers," *Damping and Isolation, Proceedings of SPIE Conference on Smart Materials and Structures, Vol. 4331*, Ed. Daniel J. Inman, pp. 82-91, 2001.

24. Choi, Y. T. and Wereley, N. M., "Assessment of Time Response Characteristics of Electrorheological and Magnetorheological Dampers," *Proceedings of SPIE, Vol. 4331,* pp. 92-102, 2001.

25. Carlson, J. D., and Spencer, B. F., Jr., "Magneto-rheological fluid dampers: Scalability and design issues for application to dynamic hazard mitigation," *Proceedings of the 2nd International Workshop on Structural Control,* Hong Kong, pp. 99-109, December, 1996.

26. Kelso, S. P., "Experimental Characterization of Commercially Practical Magnetorheological Fluid Damper Technology," *Proceedings of SPIE, Vol. 4332,* pp. 292- 299, 2001.

27. Sunakoda, K., Sodeyama, H., Iwata, N., Fujitani, H. and Soda, S., "Dynamic Characteristics of Magneto-Rheological Fluid Damper," *Proceedings of SPIE, Vol. 3989,* pp. 194-203, 2000.

28. Muriuki, M. and Clark, W., "Design Issues in Magnetorheological Fluid Actuators," *Proceedings of SPIE: Damping and Isolation, Vol. 3672,* pp. 55-64, 1999.

29. Bajkowski, J., "Modeling of shock absorbers with dry friction subjected to impact loads," *Machine Dynamics Problems, Vol. 16,* pp. 7-19, 1996.

30. Tanaka, N. and Kikushima, Y., "Impact Vibration Control Using a Semi-Active Damper," *Journal of Sound and Vibration, Vol. 158*, No. 2, pp. 277-292, 1992.

31. Johnson, N. L., Browne, A. L., "Dynamic Crush Tests Using a 'Free-Flight' Drop Tower: Theory," ET1193, General Motors R&D Center, Michigan, 2002.

32. Johnson, N. L., Browne, A. L., "Dynamic Crush Tests Using a 'Free-Flight' Drop Tower: Practical Aspects," ET1194, General Motors R&D Center, Michigan, 2002.

33. NO AUTHOR. *Building your Own Photogate Trigger.* (1999): n. pag. Online. Internet. Available: http://www.hiviz.com/tools/triggers/pg, 2003.